

# New Physics Searches at the Tevatron and the LHC\*

**André Sopczak**

Lancaster University

E-mail: [andre.sopczak@cern.ch](mailto:andre.sopczak@cern.ch)

**Abstract.** The Tevatron Run-II started data-taking in spring 2001 and several searches for new particles have been performed. The preliminary 2005 results are concisely reviewed for the experiments CDF and DØ. Model-independent and model-dependent limits on Higgs boson and Supersymmetric particle production are set and interpretations are given. Several limits from the LEP era have been extended. The outlook for the Tevatron and the prospects for the ATLAS and CMS experiments at the LHC for selected searches are briefly addressed.

PACS numbers: 14.80.Bn, 14.80.Cp, 14.80.Ly

arXiv:hep-ph/0605236v1 22 May 2006

\* Presented at PHENO 05: World Year of Phenomenology, University of Wisconsin-Madison, May 2-4, 2005; and Collider Physics Workshop: From the Tevatron to the LHC to the Linear Collider, Aspen Center for Physics, Summer 2005.

<b>1</b>	<b>Introduction</b>	<b>3</b>
<b>2</b>	<b>Higgs Boson Searches at the Tevatron</b>	<b>6</b>
2.1	Production and Decay . . . . .	6
2.2	b-Quark Tagging . . . . .	6
2.3	Gluon Fusion $gg \rightarrow H$ . . . . .	9
2.3.1	$gg \rightarrow H (H \rightarrow WW)$ . . . . .	9
2.4	Associated Production . . . . .	10
2.4.1	$WH (H \rightarrow b\bar{b})$ . . . . .	10
2.4.2	$WH (H \rightarrow WW)$ . . . . .	10
2.4.3	$ZH \rightarrow \nu\bar{\nu}b\bar{b}$ . . . . .	12
2.5	Summary of SM Higgs Cross Section Limits . . . . .	13
2.6	Beyond the SM . . . . .	15
2.6.1	$b\bar{b}h, b\bar{b}H$ and $b\bar{b}A$ in the General 2-Doublet Higgs Model or MSSM	15
2.6.2	$h, H, A \rightarrow \tau^+\tau^-$ . . . . .	16
2.6.3	$t \rightarrow H^+b$ . . . . .	17
2.6.4	$H \rightarrow \gamma\gamma$ . . . . .	19
2.6.5	$H^{++}$ . . . . .	19
<b>3</b>	<b>Supersymmetric Particle Searches at the Tevatron</b>	<b>19</b>
3.1	Di-photon (GMSB Interpretation) . . . . .	20
3.2	Tri-Lepton Signatures . . . . .	21
3.3	Scalar Quarks and Gluinos . . . . .	21
3.4	Scalar Tops and Scalar Bottoms . . . . .	22
3.5	Charged Massive Particles . . . . .	23
<b>4</b>	<b>LHC Prospects</b>	<b>25</b>
4.1	SM Higgs Boson . . . . .	25
4.1.1	Production and Decay . . . . .	25
4.1.2	Sensitivity Reach . . . . .	25
4.1.3	Parameter Determination . . . . .	26
4.2	Beyond the SM . . . . .	27
4.2.1	Invisibly Decaying Higgs Bosons . . . . .	27
4.2.2	$H \rightarrow \tau^+\tau^-$ and $\tan\beta$ Determination . . . . .	27
4.3	Supersymmetric Particles . . . . .	28
<b>5</b>	<b>Conclusions</b>	<b>30</b>

## 1. Introduction

The search for new particles is at the forefront of High Energy Physics. The discovery of a Higgs boson would shed light on electroweak symmetry breaking and the generation of mass in the Universe. Experimental evidence for Supersymmetric particles would be of equal importance and extend the Standard Model (SM) of particle physics. Many searches for new particles were performed at LEP and stringent limits on Higgs bosons in the SM and beyond were set. These limits are summarized in Table 1 (from [1]) and new model-independent limits and benchmark results in the Minimal Supersymmetric extension of the SM were recently presented [2]. The interpretations of the MSSM results depend significantly on the top quark mass. Results are presented for various top quark masses and the current (summer'05) value is  $m_t = 172.7 \pm 2.9$  GeV [3]. In addition to the limits from direct searches, some indication on the Higgs boson mass exist from precision electro-weak measurements, as shown in Fig. 1 (from [4]). About  $300 \text{ pb}^{-1}$  of data have been analyzed so far by each Tevatron experiment, while above  $1 \text{ fb}^{-1}$  data have been recorded. Figure 2 (from [5]) shows the delivered luminosity and its expectations.

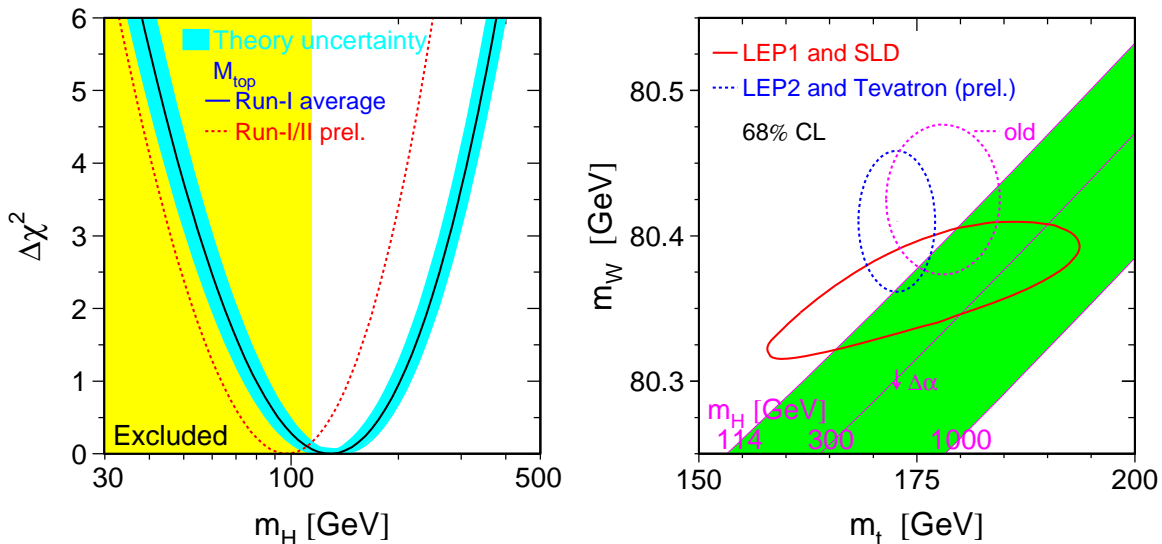


**Figure 1.** Left: Higgs boson mass prediction in the SM framework. The shift to a lower value (dotted line) from the new top quark mass measurement at the Tevatron Run-II is clearly visible. Right: old (pre-summer'05) results and the new smaller ellipse (dashed lines) prefer a region outside the SM Higgs boson mass band ( $m_H = 114$  to  $1000$  GeV). The combined results from LEP-1 and SLD are shown separately (solid line).

The Higgs boson searches at the Tevatron are discussed in Sec. 2. In Sec. 2.1 Higgs boson production and decay is addressed. Aspects of b-quark tagging are summarized in Sec. 2.2. The gluon fusion process  $gg \rightarrow H$  ( $H \rightarrow WW$ ) is presented in Sec. 2.3.

Subsequently, the associated production processes  $WH$  ( $H \rightarrow b\bar{b}, WW$ ) and  $ZH \rightarrow \nu\bar{\nu}b\bar{b}$  are discussed in Sec. 2.4. A summary of the cross section limits is given in Sec. 2.5. The following Higgs boson searches beyond the SM are presented in Sec. 2.6:  $b\bar{b}A$ ,  $A \rightarrow \tau^+\tau^-$ ,  $H \rightarrow \gamma\gamma$ ,  $t \rightarrow H^+b$ , and  $H^{++}$ . Supersymmetric particle searches at the Tevatron are reviewed in Sec. 3. First, the di-photon process in the GMSB interpretation is addressed in Sec. 3.1, then tri-lepton signatures (Sec. 3.2), scalar quarks and gluinos (Sec. 3.3), scalar tops and scalar bottoms (Sec. 3.4) and charged massive particles (Sec. 3.5). For the LHC, the prospects are briefly discussed in Sec. 4, first, for the SM Higgs boson (Sec. 4.1), then for Higgs boson searches beyond the SM (Sec. 4.2) and for Supersymmetric particles (Sec. 4.3).

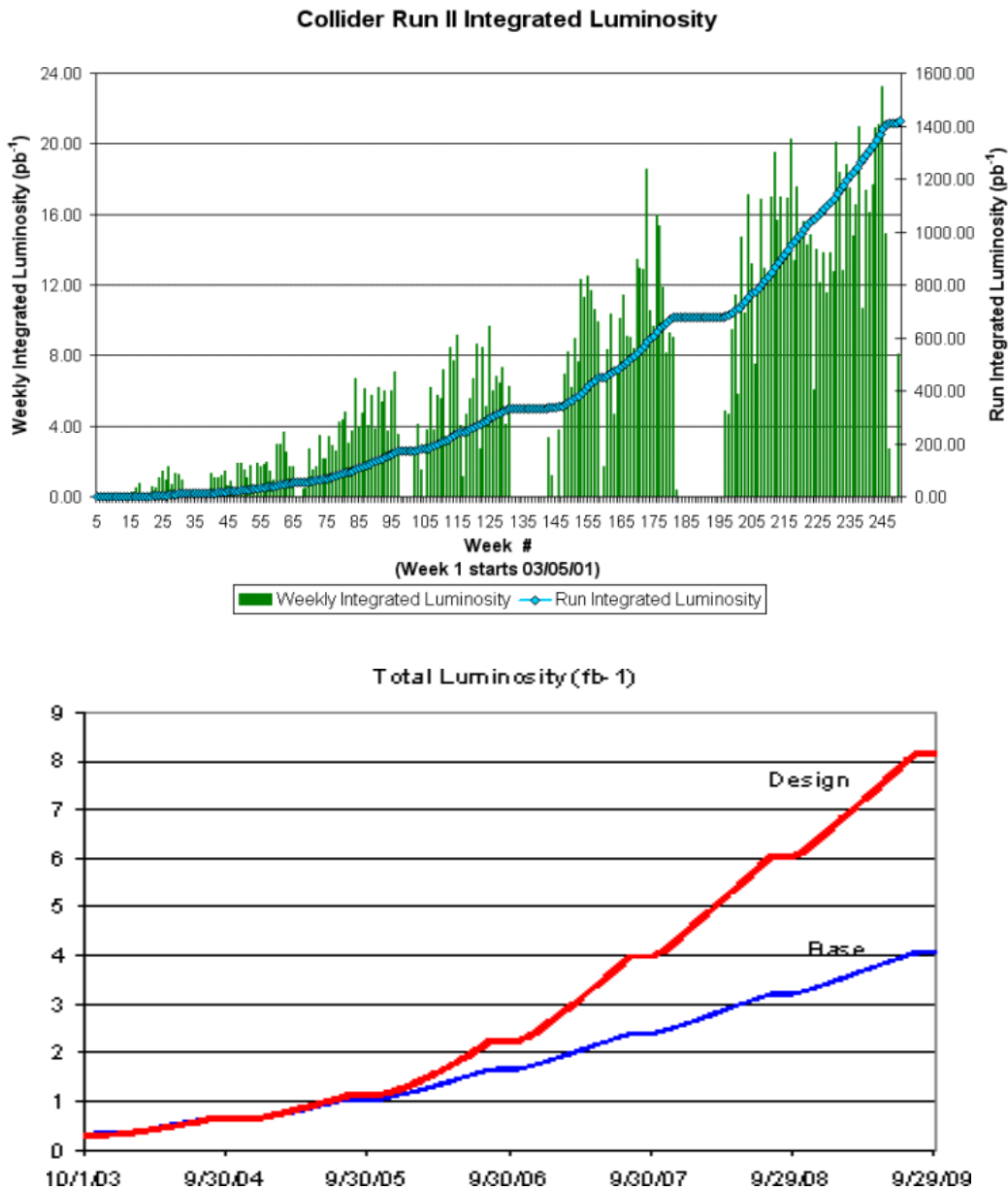


**Figure 2.** Upper: delivered Tevatron luminosity. Lower: expected integrated delivered luminosity.

**Table 1.** Summary of Higgs boson mass limits at 95% CL. ‘LEP’ indicates a combination of the results from ALEPH, DELPHI, L3 and OPAL. If results from the experiments are not (yet) combined, examples which represent the different search areas from individual experiments are given. Details of the limit parameters are given in Ref. [1].

Search	experiment	limit
Standard Model	LEP	$m_{\text{H}}^{\text{SM}} > 114.4 \text{ GeV}$
Reduced rate and SM decay		$\xi^2 > 0.05 : m_{\text{H}} > 85 \text{ GeV}$
		$\xi^2 > 0.3 : m_{\text{H}} > 110 \text{ GeV}$
Reduced rate and $b\bar{b}$ decay		$\xi^2 > 0.04 : m_{\text{H}} > 80 \text{ GeV}$
		$\xi^2 > 0.25 : m_{\text{H}} > 110 \text{ GeV}$
Reduced rate and $\tau^+\tau^-$ decay		$\xi^2 > 0.2 : m_{\text{H}} > 113 \text{ GeV}$
Reduced rate and hadronic decay		$\xi^2 = 1 : m_{\text{H}} > 112.9 \text{ GeV}$
	ALEPH	$\xi^2 > 0.3 : m_{\text{H}} > 97 \text{ GeV}$
	L3	$\xi^2 > 0.04 : m_{\text{H}} \approx 90 \text{ GeV}$
Anomalous couplings	L3	$d, d_{\text{B}}, \Delta g_1^Z, \Delta \kappa_\gamma$ exclusions
MSSM (no scalar top mixing)	LEP	almost entirely excluded
General MSSM scan	DELPHI	$m_{\text{h}} > 87 \text{ GeV}, m_{\text{A}} > 90 \text{ GeV}$
Larger top-quark mass	LEP	strongly reduced $\tan \beta$ limits
MSSM with CP-violating phases	LEP	strongly reduced mass limits
Visible/invisible Higgs decays	DELPHI	$m_{\text{H}} > 111.8 \text{ GeV}$
Majoron model (max. mixing)		$m_{\text{H,S}} > 112.1 \text{ GeV}$
Two-doublet Higgs model (for $\sigma_{\text{max}}$ )	DELPHI	$\text{hA} \rightarrow \text{b}\bar{\text{b}}\text{b}\bar{\text{b}} : m_{\text{h}} + m_{\text{A}} > 150 \text{ GeV}$
		$\tau^+\tau^-\tau^+\tau^- : m_{\text{h}} + m_{\text{A}} > 160 \text{ GeV}$
		$(\text{AA})\text{A} \rightarrow 6\text{b} : m_{\text{h}} + m_{\text{A}} > 150 \text{ GeV}$
		$(\text{AA})\text{Z} \rightarrow 4\text{b Z} : m_{\text{h}} > 90 \text{ GeV}$
		$\text{hA} \rightarrow \text{q}\bar{\text{q}}\text{q}\bar{\text{q}} : m_{\text{h}} + m_{\text{A}} > 110 \text{ GeV}$
Two-doublet model scan	OPAL	$\tan \beta > 1 : m_{\text{h}} \approx m_{\text{A}} > 85 \text{ GeV}$
Yukawa process	DELPHI	$C > 40 : m_{\text{h,A}} > 40 \text{ GeV}$
Singly-charged Higgs bosons	LEP	$m_{\text{H}^\pm} > 78.6 \text{ GeV}$
$\text{W}^\pm\text{A}$ decay mode	DELPHI	$m_{\text{H}^\pm} > 76.7 \text{ GeV}$
Doubly-charged Higgs bosons	DELPHI/OPAL	$m_{\text{H}^{++}} > 99 \text{ GeV}$
$\text{e}^+\text{e}^- \rightarrow \text{e}^+\text{e}^-$	L3	$h_{\text{ee}} > 0.5 : m_{\text{H}^{++}} > 700 \text{ GeV}$
Fermiophobic $\text{H} \rightarrow \text{WW}, \text{ZZ}, \gamma\gamma$	L3	$m_{\text{H}} > 108.3 \text{ GeV}$
$\text{H} \rightarrow \gamma\gamma$	LEP	$m_{\text{H}} > 109.7 \text{ GeV}$
Uniform and stealthy scenarios	OPAL	depending on model parameters

## 2. Higgs Boson Searches at the Tevatron

Figure 3 (from [6, 7]) shows the estimated discovery and exclusion potential for the SM Higgs boson at the Tevatron, and the dominant Higgs boson production diagrams. Currently about  $1 \text{ fb}^{-1}$  luminosity has been recorded per experiment. It is expected that by the end of 2006 about  $2 \text{ fb}^{-1}$  will have been recorded, and about  $8 \text{ fb}^{-1}$  by the end of 2009, corresponding to a 95% CL exclusion sensitivity up to 120 GeV and 180 GeV, respectively. With the anticipated delivered luminosity, it is particularly important to increase the expected sensitivity in the vicinity of 140 GeV.

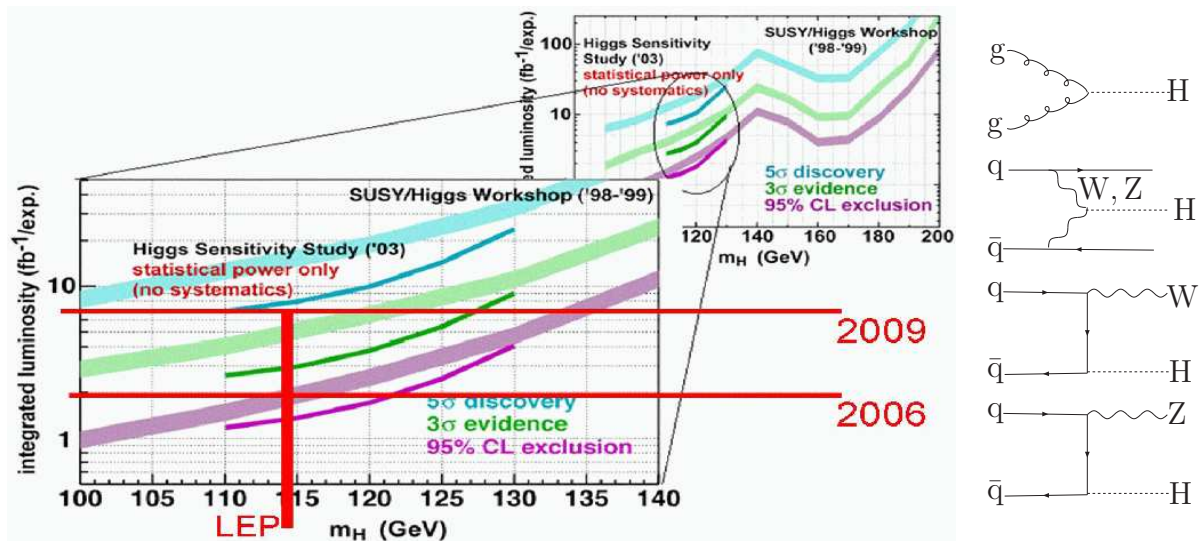


**Figure 3.** Left: expected Tevatron SM Higgs boson sensitivities from 1999 and 2003 studies. Right: Higgs boson production graphs: gluon fusion, vector boson fusion (VBF), associated production WH and WZ.

### 2.1. Production and Decay

The expected cross section and branching ratios are shown in Fig. 4 (from [8] and [9]) as a function of the Higgs boson mass. It is interesting to note that corresponding to the current collected data sample of about  $1 \text{ fb}^{-1}$  about 1000 SM Higgs bosons of 120 GeV could have already been produced at each experiment. For a SM Higgs boson mass below about 200 GeV the decay width is below 1 GeV which is much below the detector resolution.

### 2.2. *b*-Quark Tagging

The *b*-tagging capabilities are most important for the low-mass Higgs boson searches and a critical parameter is the impact parameter resolution of the vertex detector. The improvement of the impact parameter resolution with a sensitive layer very close to the interaction point is illustrated in Fig. 5 (from [12] and [13]). In CDF this layer is called L00 and in DØ it is called L0. The figure shows also the *b*-quark tagging

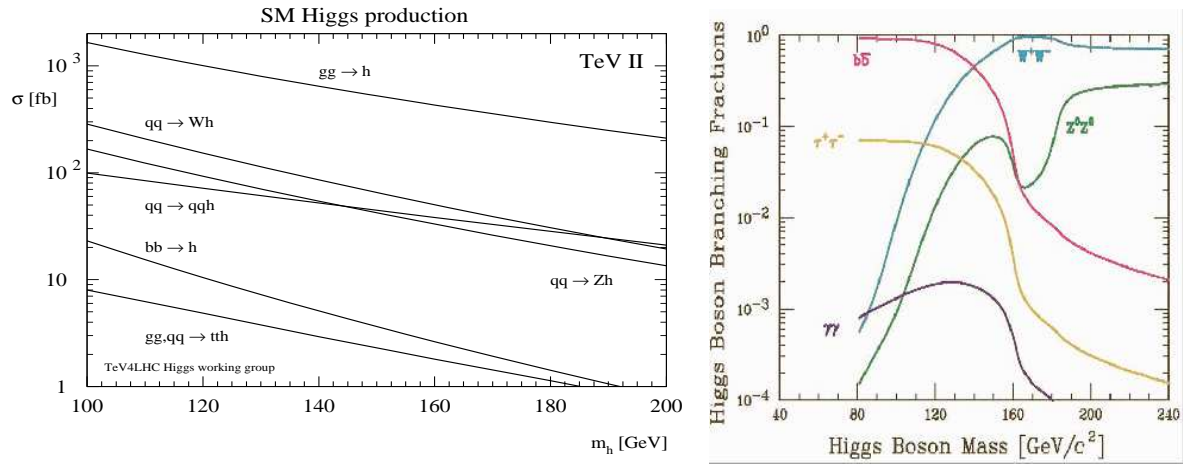


**Figure 4.** Left: expected SM Higgs boson production cross sections at the Tevatron (1.96 TeV). Right: expected Higgs boson decay branching ratios for a SM Higgs boson masses up to 240 GeV. At the Tevatron,  $b\bar{b}$  and  $WW$  decays are dominant, in addition the  $\tau^+\tau^-$  decay mode has a significant contribution.

performance [14]. An example of a quadruply b-tagged event is shown in Fig. 6 (from [15]).

Efficient B hadron tagging has already been demonstrated in data with  $Z \rightarrow b\bar{b}$  events. These measurements also contribute to the energy resolution and energy scale determinations. Figure 7 (from [10] and [11]) shows the reconstruction of the  $Z \rightarrow b\bar{b}$  mass and the good agreement between data and simulation for b-tagged  $Z$  + jets events.

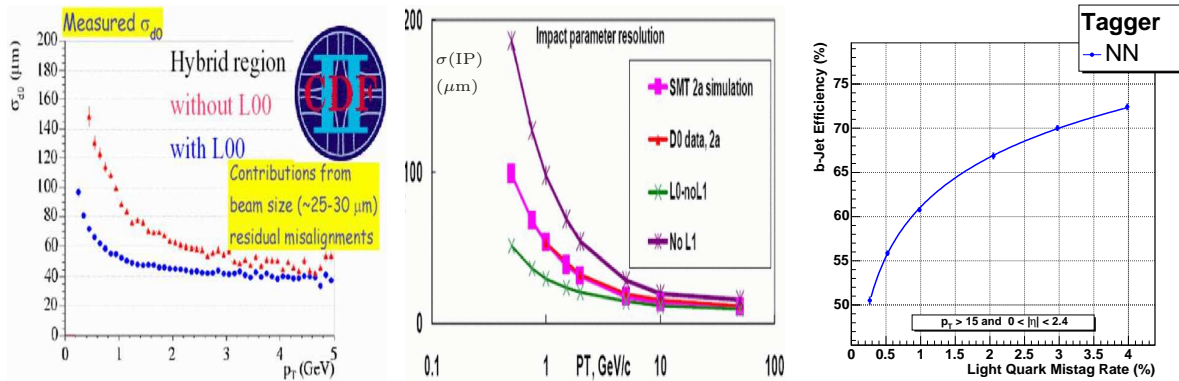


**Figure 5.** Left: CDF impact parameter resolution as a function of  $p_T$  for tracks traversing passive material in vertex detector, with (blue dots) and without (red triangles) use of L00 hits. Center: D0 expected improved impact parameter resolution with the installation of a new vertex detector layer (L0). Right: D0 b-quark tagging performance.



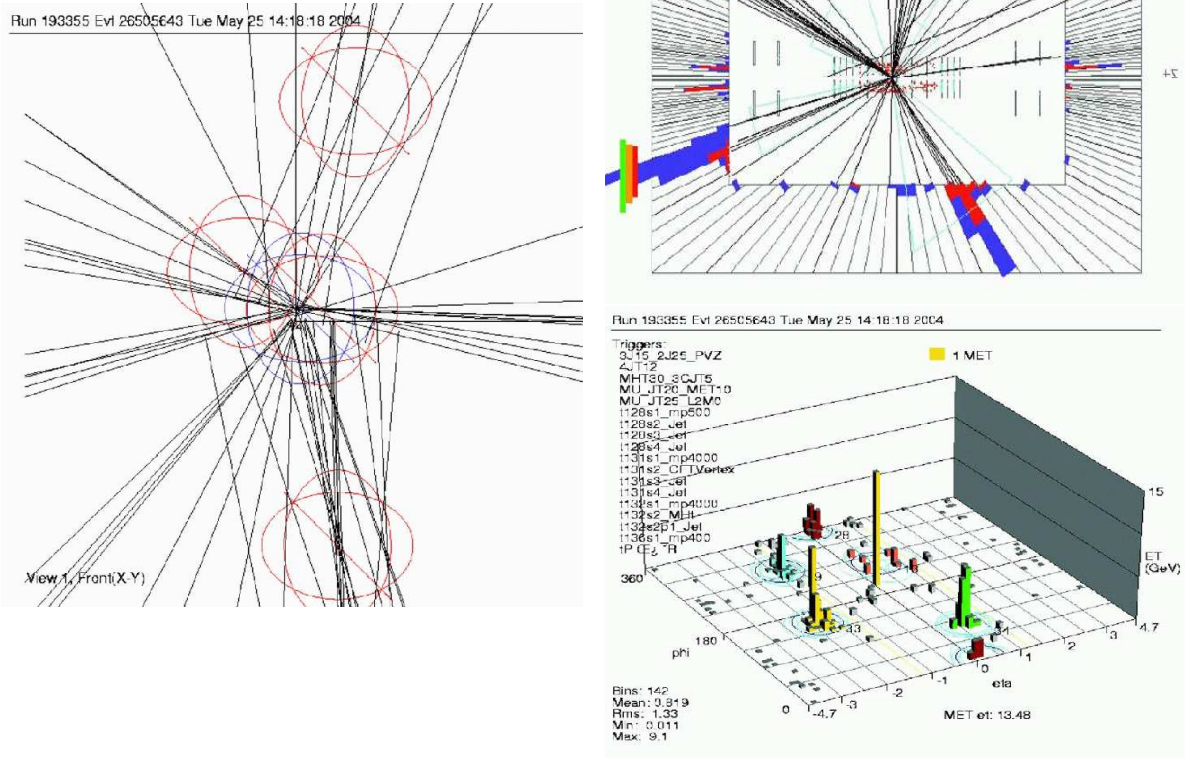


**Figure 6.**  $D\bar{0}$  example of b-tagged event. Left: reconstructed tracks near the interaction point. Upper right: jets clearly visible in the calorimeter. Lower right: jets well separated in the  $\eta$  versus  $\phi$  plane.

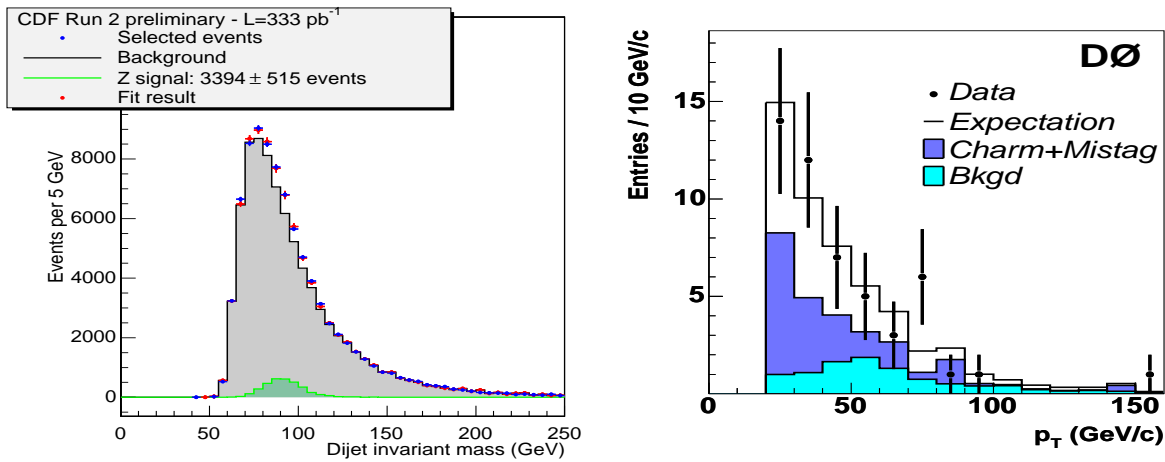


**Figure 7.** Left: CDF  $Z \rightarrow b\bar{b}$  reconstructed invariant mass for  $H \rightarrow b\bar{b}$  searches. Right:  $D\bar{0}$   $P_t$  distribution for b-tagged jets of  $Z + \text{jets}$  events.



2.3. Gluon Fusion  $gg \rightarrow H$ 

2.3.1.  $gg \rightarrow H$  ( $H \rightarrow WW$ ) For Higgs boson masses above about 135 GeV, the process  $ggH$  ( $H \rightarrow WW$ ) becomes important. The production and decay process is illustrated in Fig. 8, also shown is a background process leading to the same final state particles. The spin information allows separation of signal and background. The angle between the opposite charged leptons  $\Delta\Phi_{ll}$  tends to be smaller for the signal than for the background as shown in Fig. 8 (from [16]) and corresponding limits in Fig. 9. The good understanding of the expected background and the limits on the Higgs boson production cross section are shown in Fig. 9 (from [17] and [16]). Owing to the overwhelming  $b\bar{b}$  background, the  $gg \rightarrow H$  ( $H \rightarrow b\bar{b}$ ) channel is not feasible at the Tevatron.

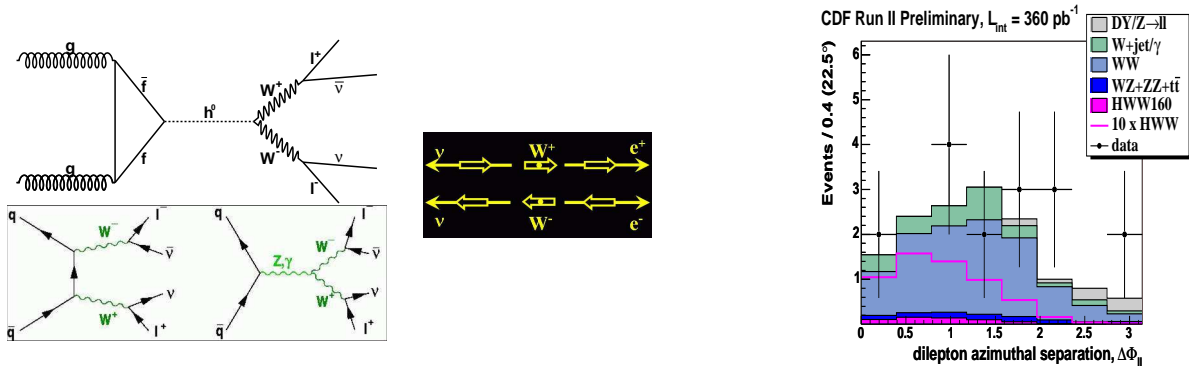


**Figure 8.** Left:  $gg \rightarrow H$  ( $H \rightarrow WW$ ) signal and background processes. Center: indication of spin correlations between final state leptons and  $W$  pairs, which lead to different dilepton azimuthal angular ( $\Delta\Phi_{ll}$ ) distributions for signal and background. Right:  $\Delta\Phi_{ll}$  distribution for data, and simulated signal and background.  $\Delta\Phi_{ll}$  is predicted to be smaller for the signal.

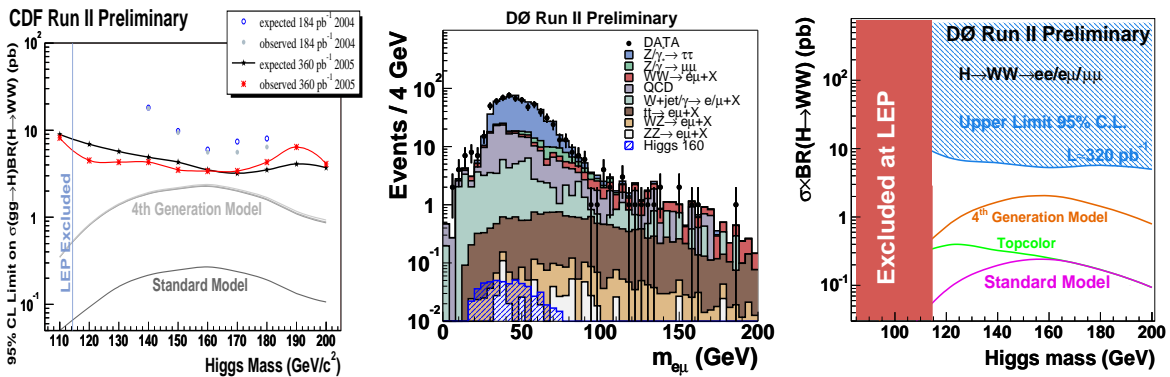


**Figure 9.** Left: CDF limits on the cross section of the  $gg \rightarrow H$  ( $H \rightarrow WW$ ) process. Center:  $D\bar{O}$  reconstructed invariant mass of  $e\mu$  pairs. Right:  $D\bar{O}$  limits on the cross section of the  $gg \rightarrow H$  ( $H \rightarrow WW$ ) process.

## 2.4. Associated Production

2.4.1.  $WH$  ( $H \rightarrow b\bar{b}$ ) An important discovery channel is the reaction  $WH$  ( $H \rightarrow b\bar{b}$ ), where the  $W$  decays either to  $e\nu$  or  $\mu\nu$ . The tagging of two  $b$ -quarks improves the signal to background ratio as shown in Fig. 10 (from [18]). Similar results are obtained from CDF, as shown in Fig. 11 (from [19]).

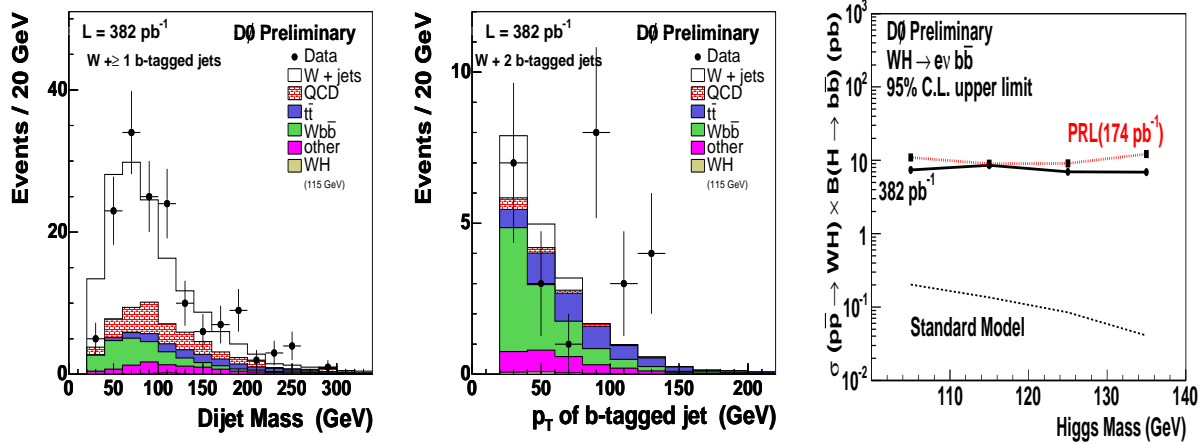


Figure 10.  $D0$   $WH$  ( $H \rightarrow b\bar{b}$ ). Left: single  $b$ -tagging. Center: double  $b$ -tagging. Right: production cross section limit.

2.4.2.  $WH$  ( $H \rightarrow WW$ ) Recent results for the search  $WH$  ( $H \rightarrow WW$ ) in the like-signed charged lepton final state are shown in Figs. 12 (from [20]) and 13 (from [21]), which lead to similar sensitivity as in the  $H \rightarrow b\bar{b}$  decay mode.

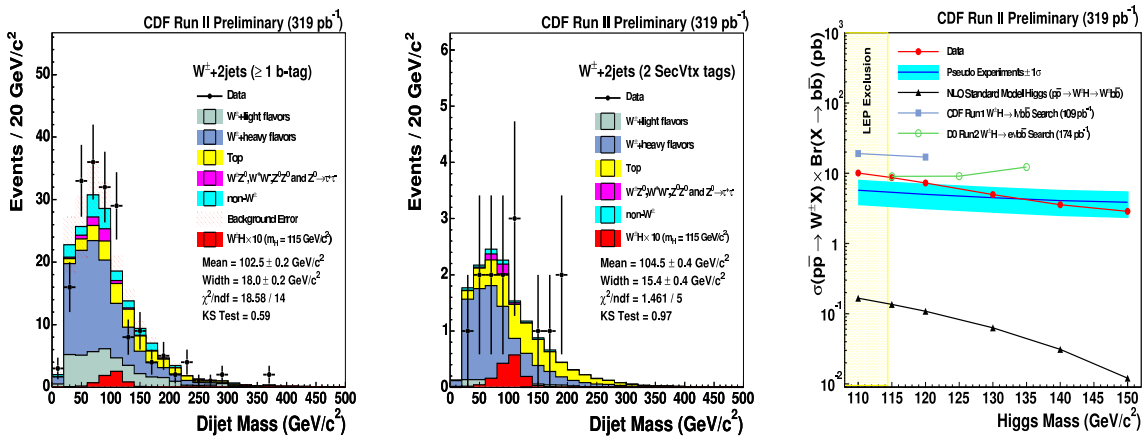


Figure 11.  $CDF$   $WH$  ( $H \rightarrow b\bar{b}$ ). Left: single  $b$ -tagging. Center: double  $b$ -tagging. Right: production cross section limit. Note that the limit is based on the single  $b$ -tagged sample which has a slightly stronger expected limited.

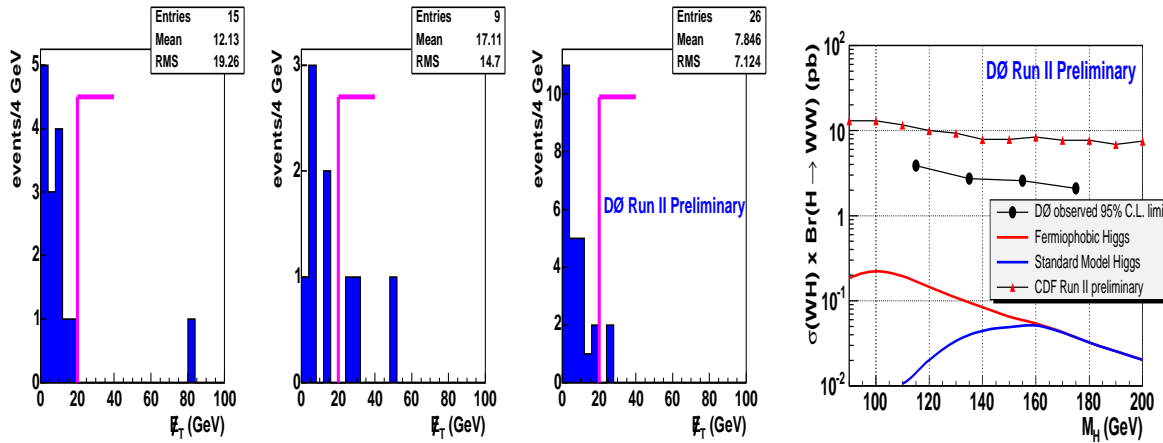


Figure 12.  $D\bar{O}$  WH ( $H \rightarrow WW$ ). Left: missing transverse energy for like-sign  $ee$  (left),  $e\mu$  (center) and  $\mu\mu$  (right). Right: cross section limit.

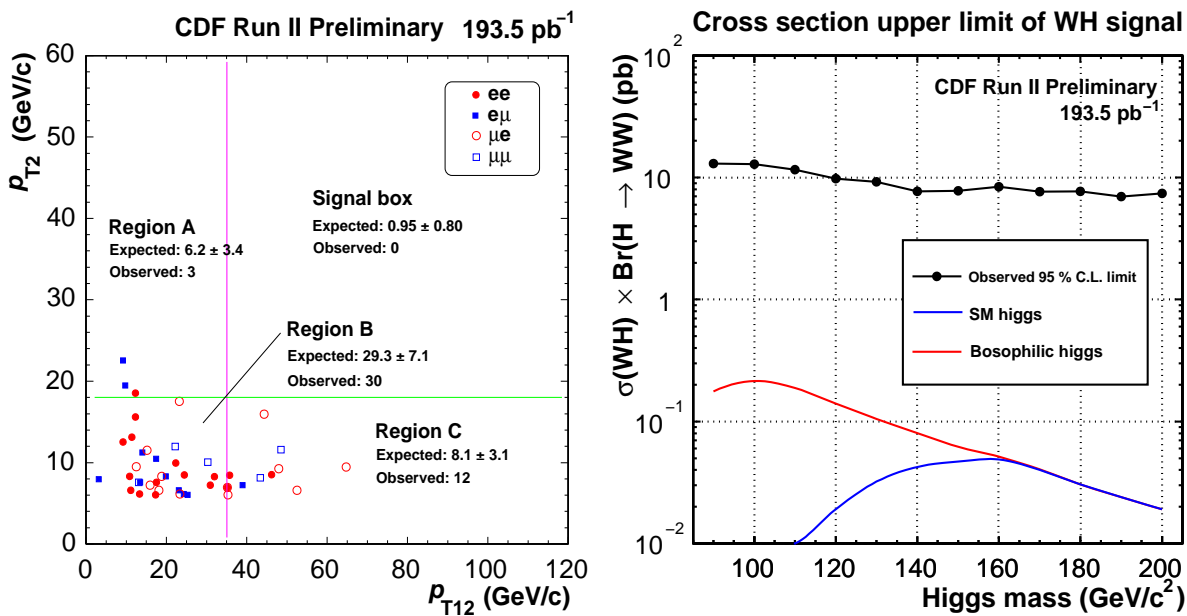


Figure 13. CDF WH ( $H \rightarrow WW$ ). Left: comparison of simulated background and observed number of events in the plane of the second most energetic lepton  $p_{T2}$  versus di-lepton vector sum  $p_{T12}$ . Right: cross section limit.

2.4.3.  $ZH \rightarrow \nu\bar{\nu}b\bar{b}$  Both Tevatron experiments have searched for a  $ZH \rightarrow \nu\bar{\nu}b\bar{b}$  signal, which has a smaller cross section compared to WH production. The results from the expected missing energy and b-jet signal are shown in Figs. 14 (from [22]) and 15 (from [23]). The CDF cross section limits are shown in Fig. 16 (from [23]).

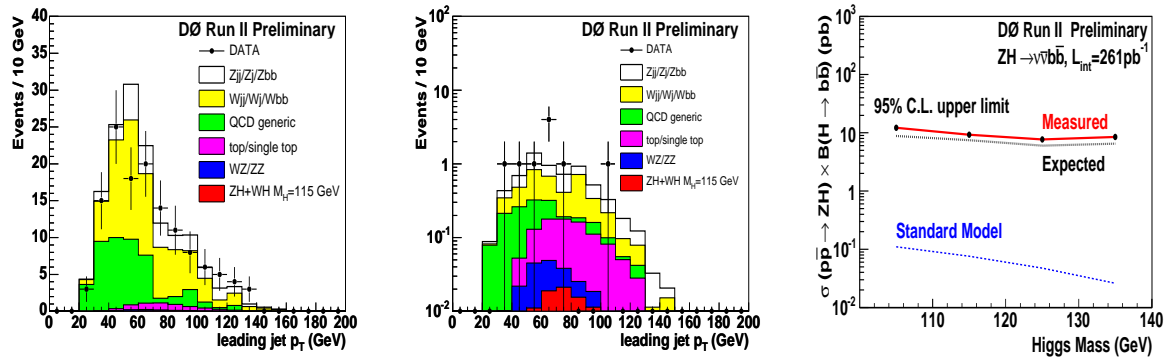


Figure 14. D0  $ZH (H \rightarrow b\bar{b})$ . Left: single b-tagging. Center: double b-tagging. Right: cross section limit.

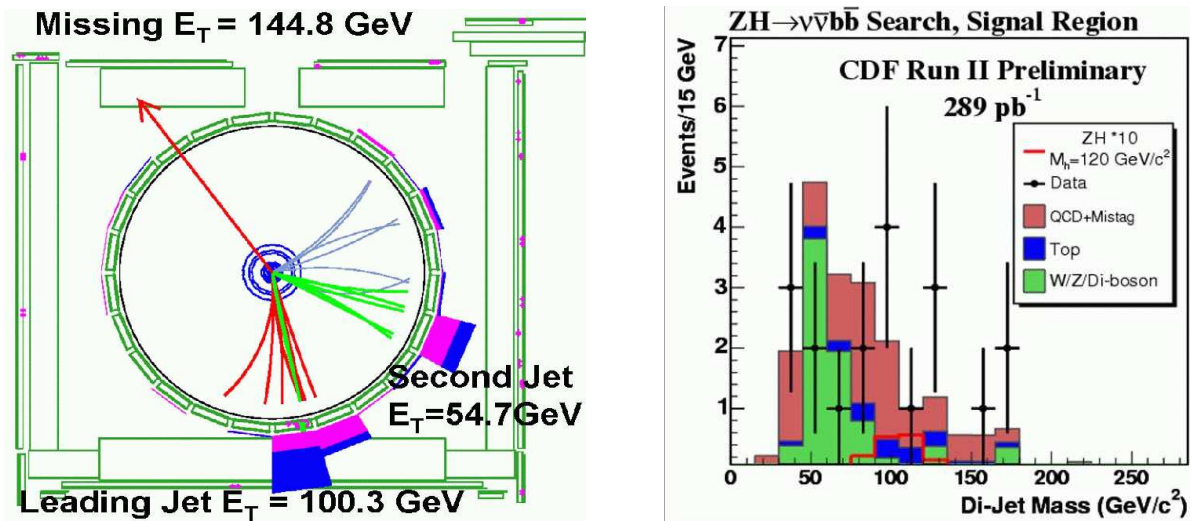


Figure 15. CDF  $ZH (H \rightarrow b\bar{b})$ . Left: candidate event. Right: di-jet mass for data and simulated signal and background.

### 2.5. Summary of SM Higgs Cross Section Limits

Cross section limits for a 120 GeV SM Higgs boson production are summarized in Table 2. At this mass the SM expectation is about  $\sigma \times \text{BR} = 0.1$  pb for the processes  $\text{WH} \rightarrow \text{Wb}\bar{\text{b}}$  and  $\text{gg} \rightarrow \text{H} \rightarrow \text{b}\bar{\text{b}}$  processes. The current CDF and DØ limits as a function of the SM Higgs boson mass are given in Fig. 16 (from [24]), and also shown are the ratios of observed cross section limits and the expected SM cross section.

**Table 2.** Summary of observed and expected limits at 95% CL from CDF and DØ for a 120 GeV SM Higgs boson. Recently, through optimizations, the expected DØ  $\nu\bar{\nu}\text{b}\bar{\text{b}}$  limit has been reduced by about a factor 2 [25].

Channel	experiment	luminosity ( $\text{pb}^{-1}$ )	limit $\sigma \times \text{BR}$ (pb)	
			obs.	exp.
$\text{H} \rightarrow \text{WW} \rightarrow \ell\nu\ell\nu$	CDF	360	4.5	6.9
	DØ	299-325	5.6	9.5
$\text{WH} \rightarrow \ell\nu\text{b}\bar{\text{b}}$	CDF	319	7.2	5.0
	DØ	382	7.8	5.7
$\text{WH} \rightarrow \text{WWW}$	CDF	194	9.7	15
	DØ	363-384	3.5	4.2
$\text{ZH} \rightarrow \nu\bar{\nu}\text{b}\bar{\text{b}}$	CDF	289	4.5	3.6
	DØ	261	8.5	6.5

These limits are about a factor two weaker compared to the estimates [6, 7] for the luminosity of about  $300 \text{ pb}^{-1}$ . Improvements will come from optimized b-quark tagging, and also from larger  $e/\mu$  acceptance, better jet mass resolution, and from using advanced analysis techniques. Higher Higgs boson sensitivities will also result from the luminosity increase over the next years. Currently already about  $1 \text{ fb}^{-1}$  is recorded per experiment, and the total luminosity will increase up to about  $8 \text{ fb}^{-1}$ . Reaching the sensitivity of LEP (114 GeV), and extending beyond, possibly to reach 180 GeV, will be a large experimental challenge over the next few years. The combination of the  $\text{H} \rightarrow \text{b}\bar{\text{b}}$  and  $\text{H} \rightarrow \text{WW}^*$  searches give lower sensitivity reduction around 140 GeV compared to the estimates shown in Fig. 3. Nevertheless, particular attention needs to be devoted to the mass region around 140 GeV for example by investigating new search reactions (e.g.  $\text{H} \rightarrow \tau\tau$  [26]) which were not included in the previous estimates [6, 7].

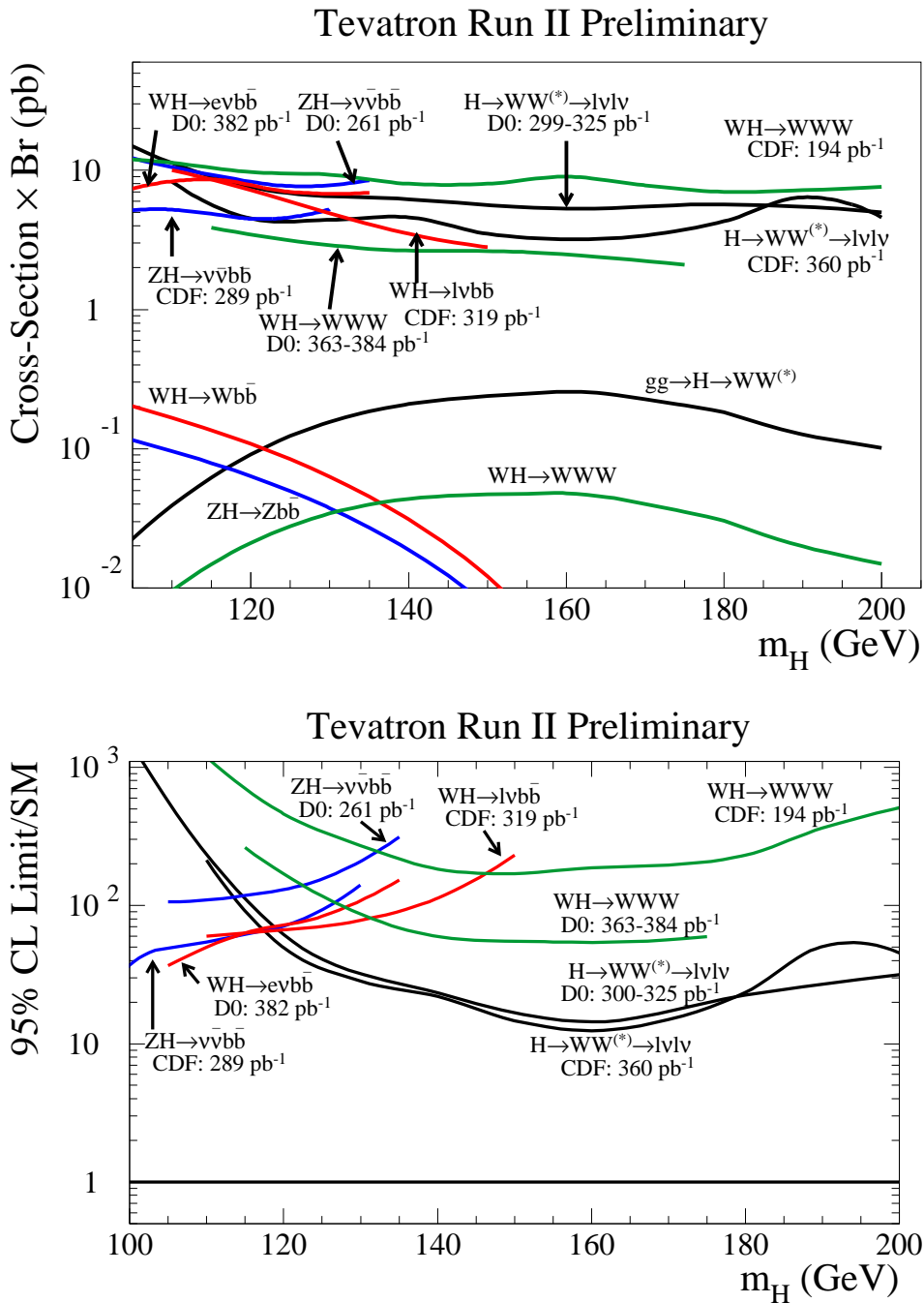


**Figure 16.** Left: summary of SM Higgs boson limits from CDF and DØ Higgs boson searches. Right: ratio of observed cross section limit and expected SM cross section.



## 2.6. Beyond the SM

**2.6.1.  $b\bar{b}h$ ,  $b\bar{b}H$  and  $b\bar{b}A$  in the General 2-Doublet Higgs Model or MSSM** Higgs boson production process in association with b-quarks in  $p\bar{p}$  collisions has been calculated in two ways: in the five-flavor scheme [27], where only one b-quark has to be present in the final state, while in the four-flavor scheme [28], two b-quarks are explicitly required in the calculation. Both calculations are now available at next-to-leading order (NLO QCD), and agree taking into account the theoretical uncertainties. Figure 17 (from [29]) illustrates these processes for h production at leading order (LO), and analogous diagrams can be drawn for the H and A bosons. The cross section depends mostly on  $\tan^2\beta$  and to a smaller extent on other Supersymmetric parameters as given by:

$$\sigma \times BR_{\text{SUSY}} \approx 2\sigma_{\text{SM}} \frac{\tan^2\beta}{(1 + \delta_b)^2} \frac{9}{9 + (1 + \delta_b)^2},$$

where  $\delta_b = k \tan\beta$  with  $k$  depending on the SUSY parameters, in particular also on  $A_t$ , the mixing in the scalar top sector, the gluino mass, the  $\mu$  parameter, stop and sbottom masses.

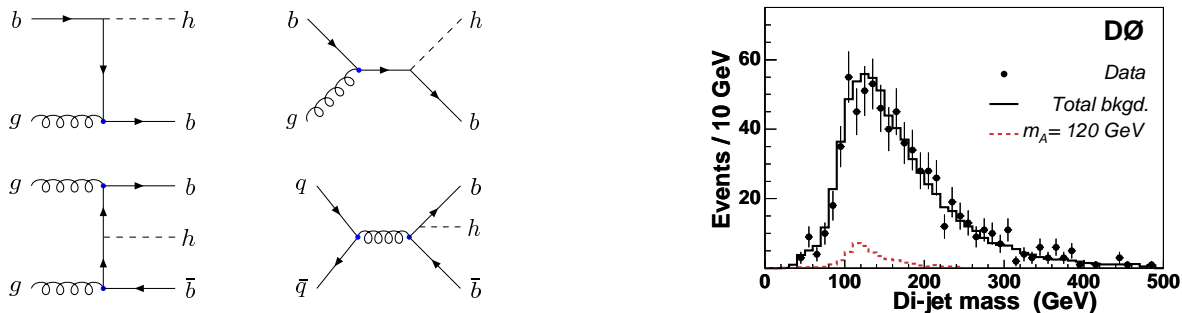


**Figure 17.** DØ. Left: leading-order Feynman diagrams for neutral Higgs boson production in the five-flavor scheme (top) and four-flavor scheme (bottom). Right: invariant mass spectrum of two leading jets in events with at least three b-tagged jets, estimated background, and the signal simulation for a 120 GeV Higgs boson that can be excluded at the 95% CL (for  $\tan\beta \approx 30$ ).

There is no indication of a  $b\bar{b}A$  production in the data (Fig. 17). The resulting limits on the production cross section, and in the MSSM are given in Fig. 18 (from [29]). Previous results by the CDF Collaboration [30] were not confirmed with the DØ data. In the CDF analysis gluon parton distribution function PDFs were used that have been superseded, resulting in more stringent limits than would have been obtained with the more recent PDFs used in the DØ analysis. Figure 18 (from [31]) includes also the sensitivity prospects for larger luminosities.

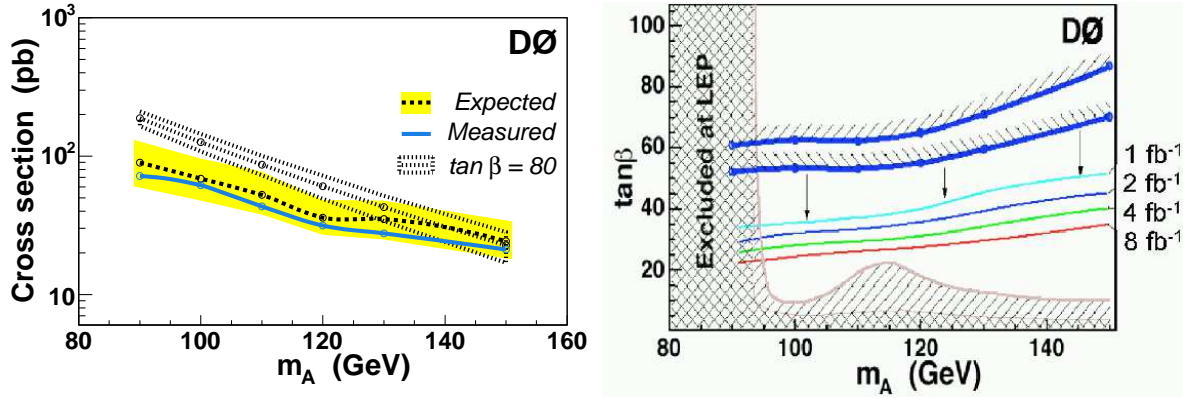


**Figure 18.** DØ. Left: expected (in absence of a signal) and measured 95% CL upper limits on the signal cross section as a function of  $m_A$ . The band indicates the  $\pm 1\sigma$  range on the expected limit. Also shown is the cross section for the signal at  $\tan\beta = 80$  in the “no mixing” scenario of the MSSM, with the theoretical uncertainty indicated by the overlaid band. Right: 95% CL upper limit on  $\tan\beta$  as a function of  $m_A$  for two scenarios of the MSSM, “no mixing” and “maximal mixing.” In addition, the expected sensitivities at 95% CL for the maximal mixing scenario are shown. The limits obtained by the LEP experiments for the same two scenarios of the MSSM are given also.

2.6.2.  $h, H, A \rightarrow \tau^+\tau^-$  The signature for  $h, H, A \rightarrow \tau^+\tau^-$  opens additional possibilities for Higgs boson discovery. The characteristic enhancement in the one- and three-track bins from hadronic  $\tau$  decays is shown in Fig. 19 (from [32]). Tau leptons are identified as isolated jets with few tracks. For  $m_A = 140$  GeV, the visible mass for a simulated background and data is shown. The background from misidentified jets, as determined by the simulation, is indicated. Resulting limits in the MSSM and production cross section limits are given in Fig. 20 (from [32]), also shown are the sensitivity prospects with larger luminosity (from [31]).

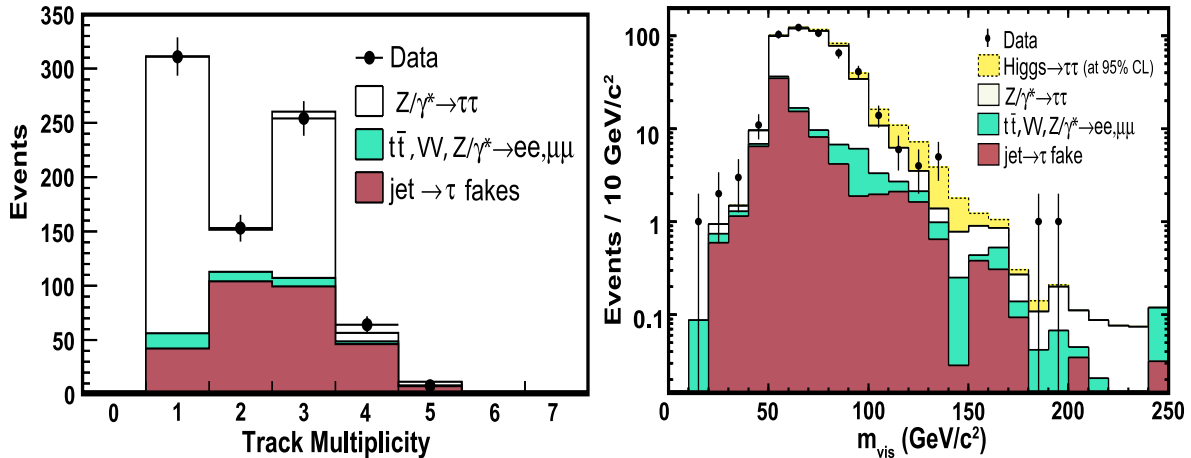


**Figure 19.** CDF. Left: track multiplicity for hadronically decaying tau candidates. Right: visible mass distribution for a simulated signal of  $m_A = 140$  GeV, background and data.

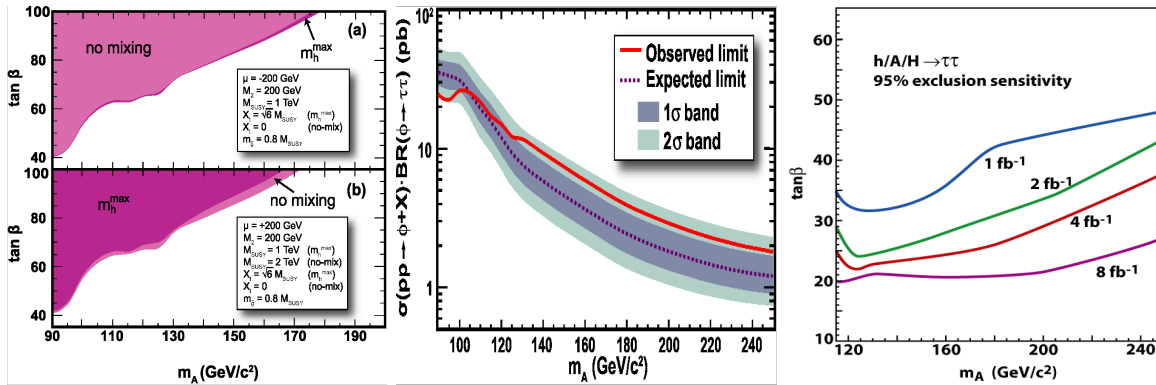


**Figure 20.** CDF. Left: excluded regions in the  $\tan\beta$  versus  $m_A$  plane for the maximum-mixing and no-mixing scenarios with (a)  $\mu < 0$  and (b)  $\mu > 0$ . Center: upper limits at 95% CL on Higgs production cross section times branching fraction to  $\tau$  pairs. Right: expected  $\tan\beta$  sensitivities for larger luminosities.

**2.6.3.  $t \rightarrow H^+b$**  The decay of top quarks  $t \rightarrow H^+b$  is possible in general Higgs boson models with two Higgs boson doublets. The expected top and charged Higgs boson branching fractions are shown in Fig. 21 (from [33]) as a function of  $\tan\beta$ . The expected SM top decay rate would be modified. No deviation from the SM top decay rates are observed (Fig. 22) and resulting limits are given in Fig. 23.

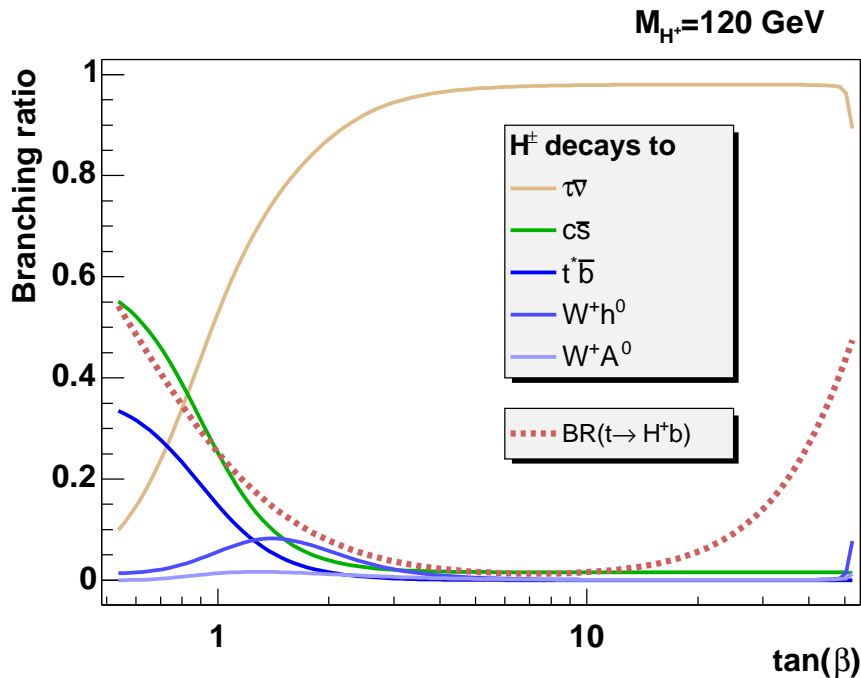


**Figure 21.** CDF. Branching ratios for a 120 GeV charged Higgs boson production in top decays and charged Higgs boson decays, which depends mostly on  $\tan\beta$  in the general 2-doublet Higgs model.

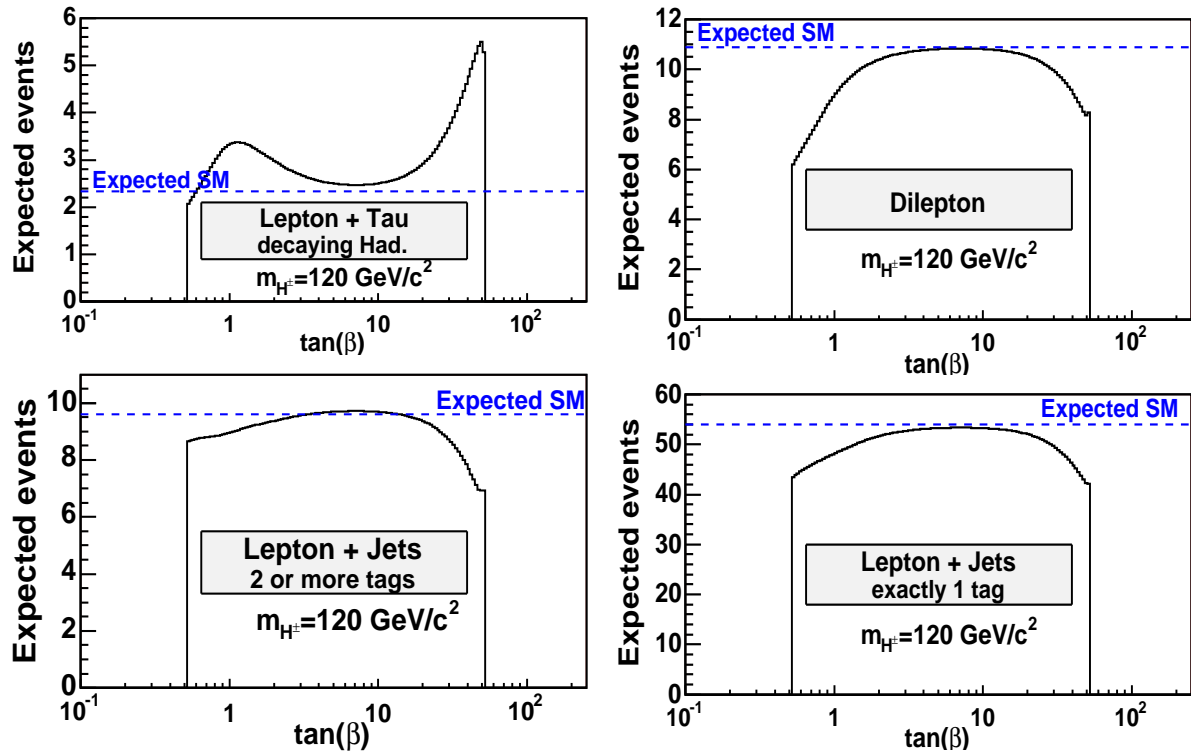


Figure 22. CDF. Expected events from top decays in different analysis channels for the SM and as function of  $\tan\beta$  for charged Higgs boson production. The numbers of data events 2, 13, 8 and 49 agree well with the SM expectations.

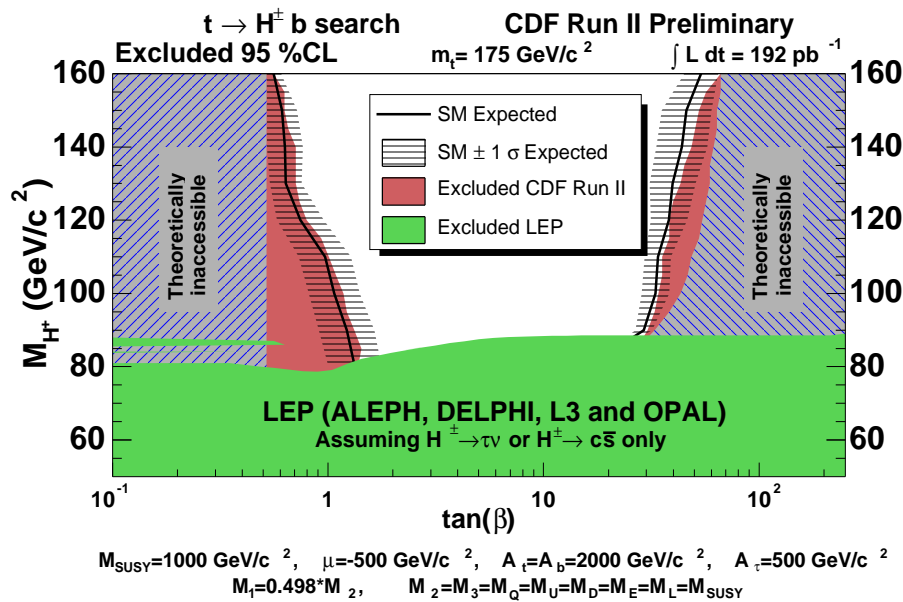


Figure 23. CDF. Limits on the charged Higgs boson mass as function of  $\tan\beta$  for a specific set of SUSY parameters.

2.6.4.  $H \rightarrow \gamma\gamma$  In fermiophobic Higgs boson models, the dominant decay mode could be  $H \rightarrow \gamma\gamma$ . No indication of a resonance has been observed in the  $\gamma\gamma$  invariant mass spectrum and limits on the  $H \rightarrow \gamma\gamma$  production are set as shown in Fig. 24 (from [34]).

2.6.5.  $H^{++}$  The possibility of doubly-charged Higgs boson exists in models with Higgs boson triplets. Pairs of like-sign charged leptons are expected from the decay of the doubly-charged Higgs bosons. No indication has been observed in the data and limits on the double charged Higgs boson mass from CDF [35] and DØ [36] are given in Fig. 24.

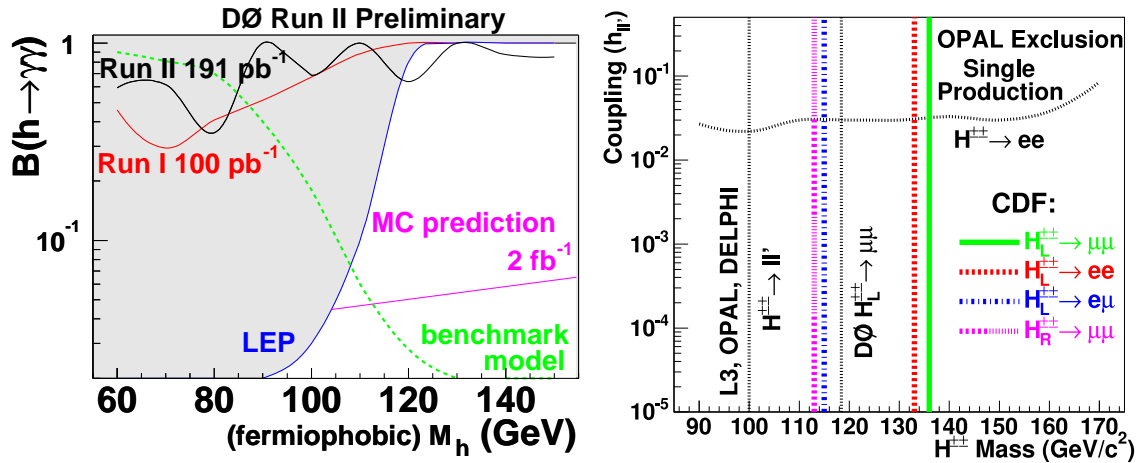
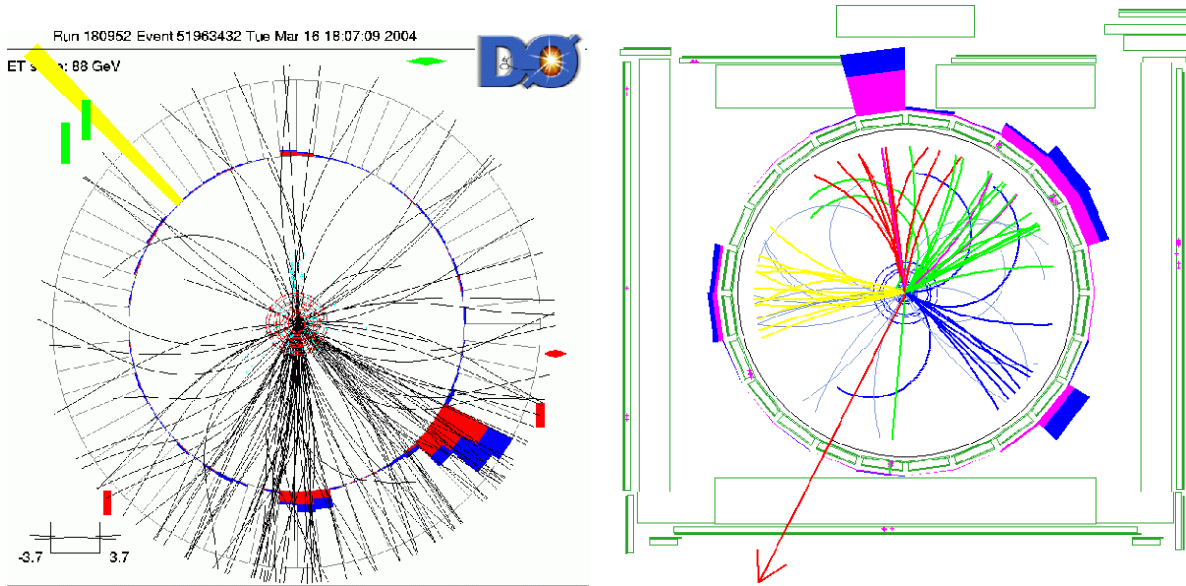


Figure 24. Left: DØ limits on  $H \rightarrow \gamma\gamma$ . Right: CDF and DØ doubly charged Higgs boson mass limits.

### 3. Supersymmetric Particle Searches at the Tevatron

In the production of Supersymmetric particles (sparticles) the lightest supersymmetric particle (LSP) is stable (if R-parity is conserved) and escapes detection, leading to missing momentum and missing energy in the recorded events. Figure 25 shows events with jets and large  $H_T$  defined as the sum of the transverse jet momenta for DØ [37] and defined as the sum of the transverse jet energies for CDF [38].

Previous combined results from the LEP experiments have set limits on several sparticles close to the kinematic reach. Figure 26 (from [39]) shows the excluded region in the  $\tan\beta$  versus LSP mass plane in the MSSM, and in the Gauge Mediated Supersymmetry Breaking (GMSB) model. The position of an intriguing CDF  $ee\gamma\gamma$  candidate event [40] from the Tevatron Run-I is indicated (dashed line) and the GMSB interpretation for this event is excluded at 95% CL.



**Figure 25.** Events with large missing momentum and energy. Left: DØ  $H_T = 410$  GeV. Right: CDF  $H_T = 404$  GeV.

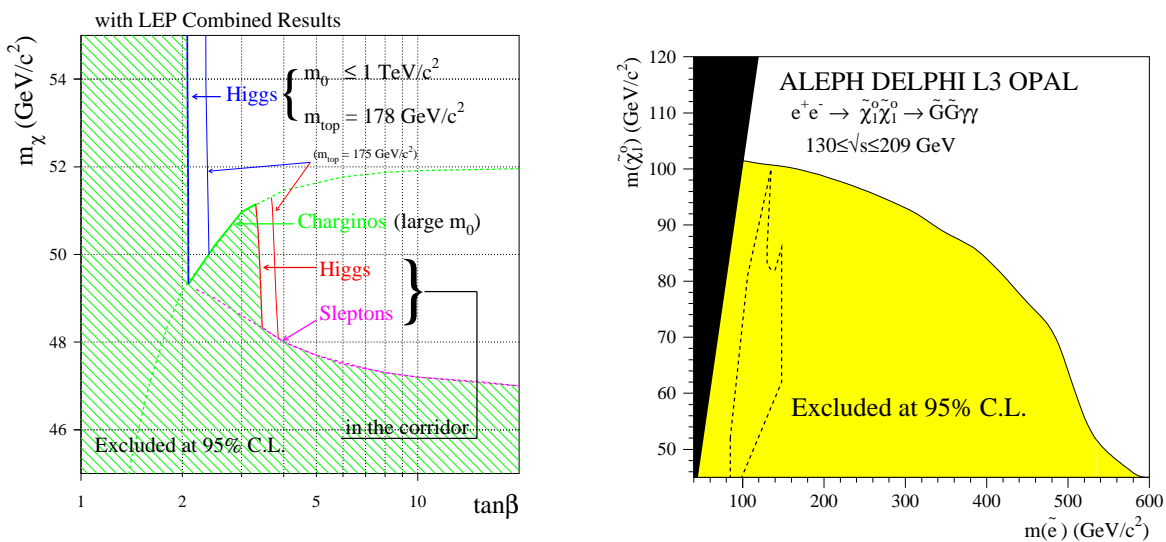


**Figure 26.** Left: combined LEP limits in the  $\tan\beta$  versus neutralino plane in a constrained MSSM. Right: combined LEP exclusion in the selectron versus neutralino plane from acoplanar photon searches. The CDF Run-I  $ee\gamma\gamma$  candidate event is indicated in the excluded region.

### 3.1. Di-photon (GMSB Interpretation)

In the GMSB model, chargino-neutralino production has been searched for by CDF and DØ. The production reaction is illustrated in Fig. 27 (from [41]). The figure shows also that the expected signal and background can be well separated. There is no indication of a signal in the data and the combined limits on the chargino mass from CDF and DØ are given [42].



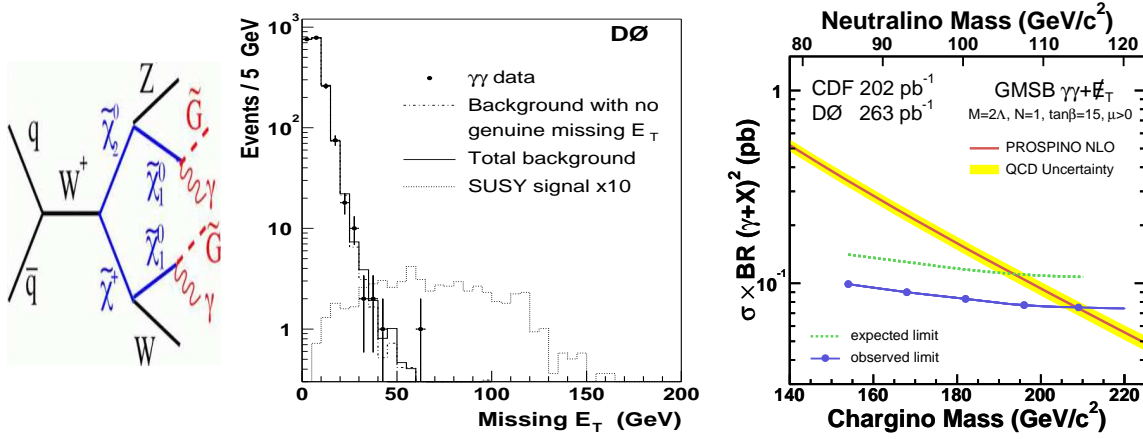


**Figure 27.**  $D\bar{0}$  GMSB. Left: production graph. Center: missing transverse energy. Right: combined CDF and  $D\bar{0}$  exclusion.

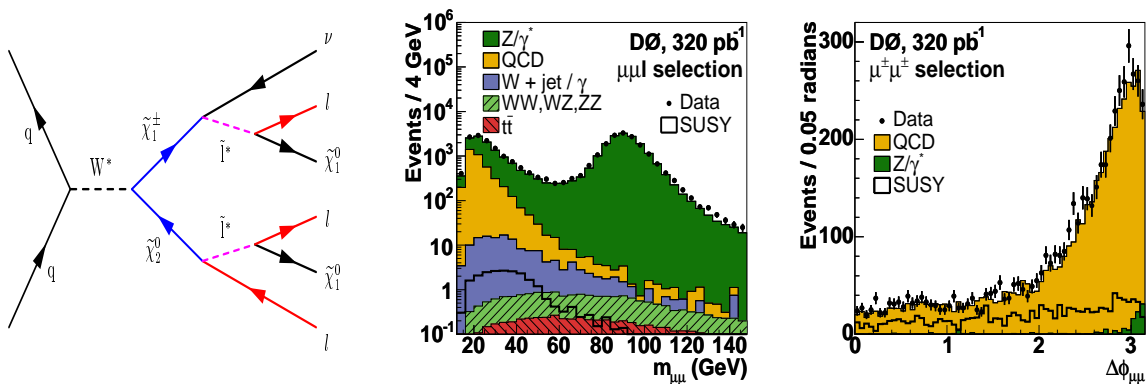


**Figure 28.**  $D\bar{0}$ . Left: tri-lepton production graph. Center: invariant di-muon mass  $m_{\mu\mu}$ . Right: di-muon opening angle  $\Delta\phi_{\mu\mu}$  for data, background and simulated signal.

### 3.2. Tri-Lepton Signatures

The sparticle production with a tri-lepton final state is illustrated in Fig. 28. Figures 28, 29, and 30 (from [43]) show the good agreement between data and simulated background for various final states with a tri-lepton signatures. There is no indication of a signal and resulting limits are given as a function of the chargino mass. With increasing luminosities 1, 2, 4, 8  $\text{fb}^{-1}$  and for a scenario with maximal leptonic branching ratio, the expectations for the chargino mass reach are 170, 210, 235 and 265 GeV, as shown in Fig. 30 (from [44]).

### 3.3. Scalar Quarks and Gluinos

Depending on the masses of squarks and gluinos, either  $\tilde{q}\tilde{q}^*$ ,  $\tilde{g}\tilde{g}^*$ , or  $\tilde{q}\tilde{g}^*$  could be produced. For gluinos heavier than squarks, squark pair-production dominates, leading to a signature of two acoplanar jets and missing energy from the escaping neutralino. If the squarks are heavier than gluinos, gluino pair-production is expected, leading to four, and more, jets. If both masses are about equal, squark-gluino production is expected.

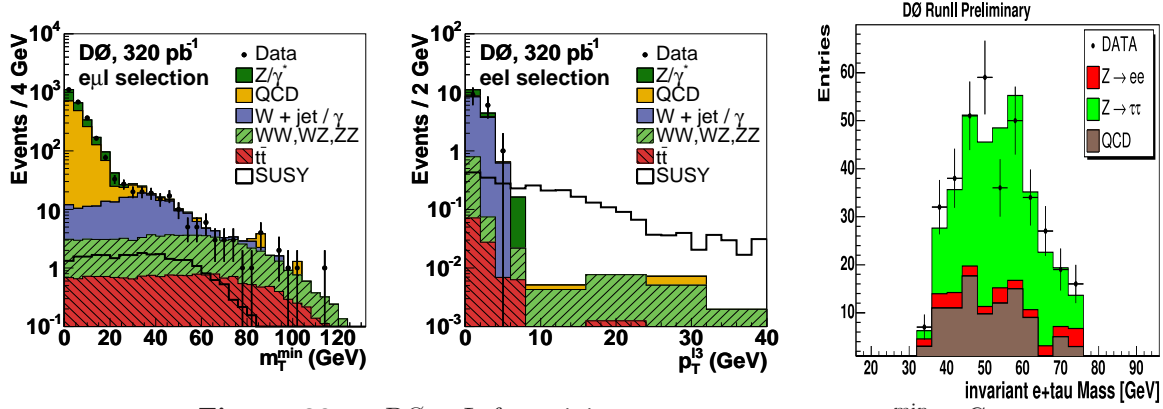


Figure 29. DØ. Left: minimum transverse mass  $m_T^{\min}$ . Center: transverse momentum of the third track  $p_T^3$  for data, background and simulated signal. Right: invariant mass of  $e\tau$ .

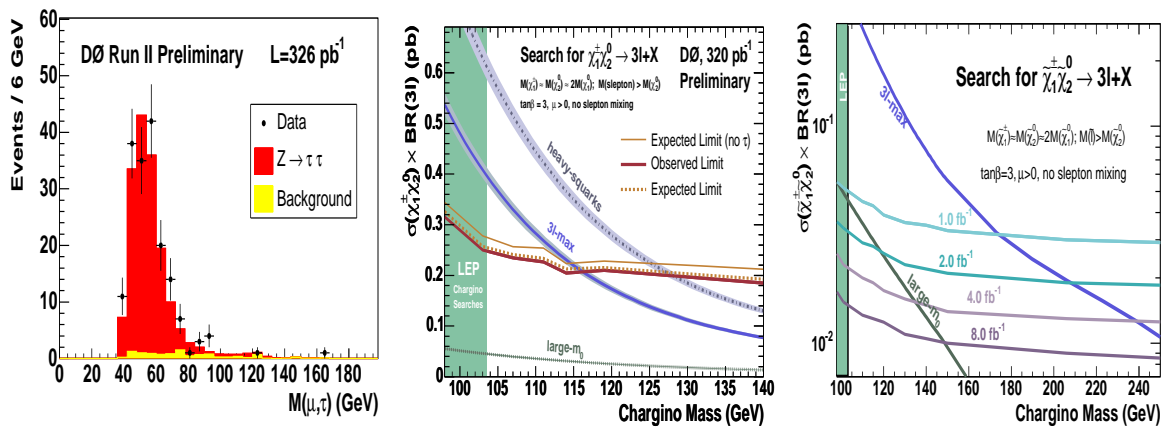


Figure 30. DØ. Left: invariant mass of  $\mu\tau$ . Center: limits from the tri-lepton searches. Right: sensitivity expectations from the tri-lepton searches with larger luminosities.

Figures 31 and 32 (from [37]) show the missing  $E_T$  distributions for expected signal and background in the three cases, and also the resulting mass limits and future sensitivity expectations [44].

### 3.4. Scalar Tops and Scalar Bottoms

The pair-production of light scalar top quarks is characterized by two c-quark jets and missing energy if the decay into  $b\chi^\pm$  is kinematically suppressed. Currently the experimental cross section sensitivity approaches the expected signal cross section. More luminosity is required to reach sensitivity for the scalar top mass of up to about 160 to 180 GeV, as shown in Fig. 33 (from [45]). A minimum stop-neutralino mass difference of about at least 35 GeV is required, unlike LEP [39] or the ILC [46], where also small mass differences are covered. In addition, the search for the reaction  $\tilde{t}_1 \tilde{t}_1 \rightarrow b\bar{b}\mu^+\mu^-\tilde{\nu}\tilde{\nu}$  has been performed and resulting limits are shown also in Fig. 33 (from [47]).

Two b-jets and missing energy from the neutralinos are expected in the final state of sbottom pair-production. The missing  $E_T$  and mass limits in the sbottom-neutralino

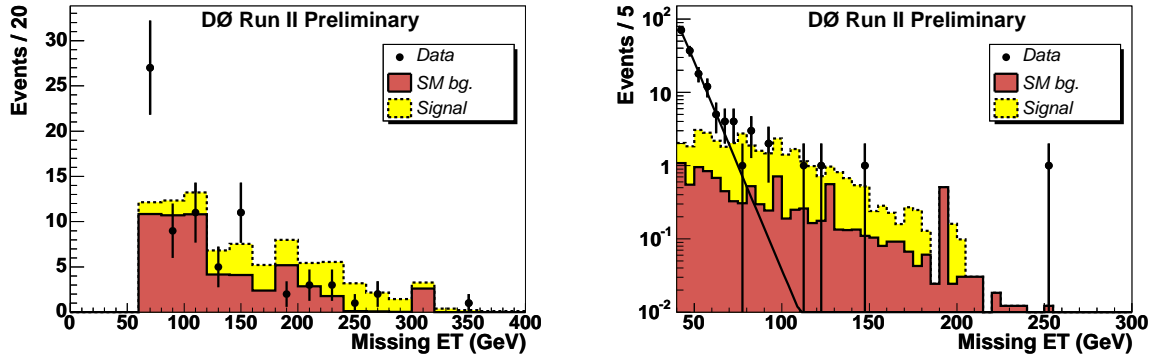


**Figure 31.**  $D\bar{O}$ . Left: gluino heavier than squark, squark pair-production is expected, leading to acoplanar di-jets. The excess at low missing  $E_T$  is due to QCD background. Right: squark heavier than gluino, gluino pair-production is expected, leading to four and more jets.

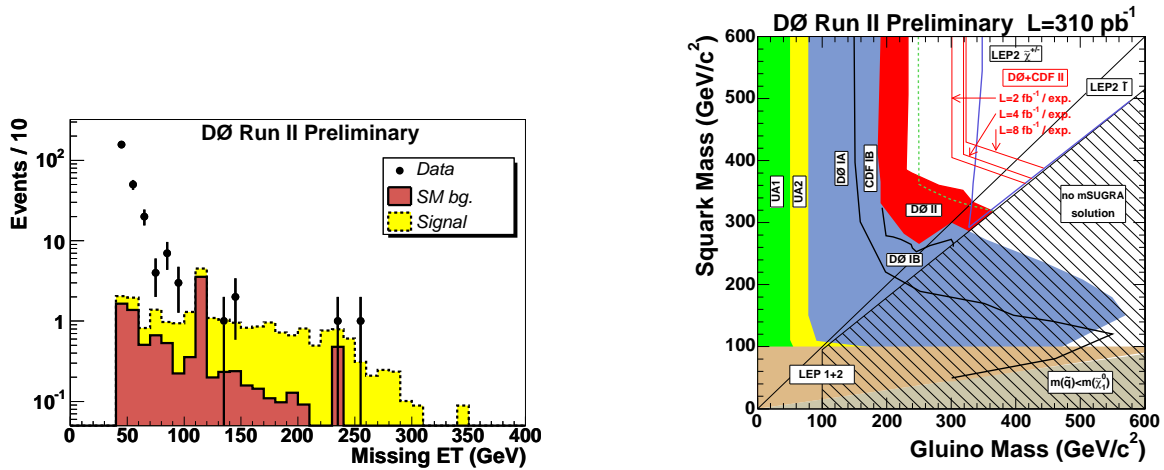


**Figure 32.**  $D\bar{O}$ . Left: gluino and squark masses are about equal, squark-gluino production is expected, leading typically to three jets. The excess at low missing  $E_T$  is due to QCD background. Right: squark-gluino mass limits. With the current luminosity, only a small region beyond the LEP limits near the diagonal is excluded. The sensitivity reach with larger luminosities is also shown.

plane are shown in Fig. 34 (from [48]).

### 3.5. Charged Massive Particles

The production of stable scalar tau leptons would lead to a signature in the detector like a pair of muons, but with invariant mass and speed inconsistent with the production of muon pairs. The expected speed of these charged massive particles is expected to be significantly different compared to muons as shown in Fig. 35 (from [49]). An interpretation of the results as limits on chargino masses are given in the nearly mass-degenerate neutralino-chargino scenario, which occurs naturally in the Anomaly Mediated Symmetry Breaking (AMSB) model. Also shown is an example in the MSSM when the chargino is Higgsino-like.

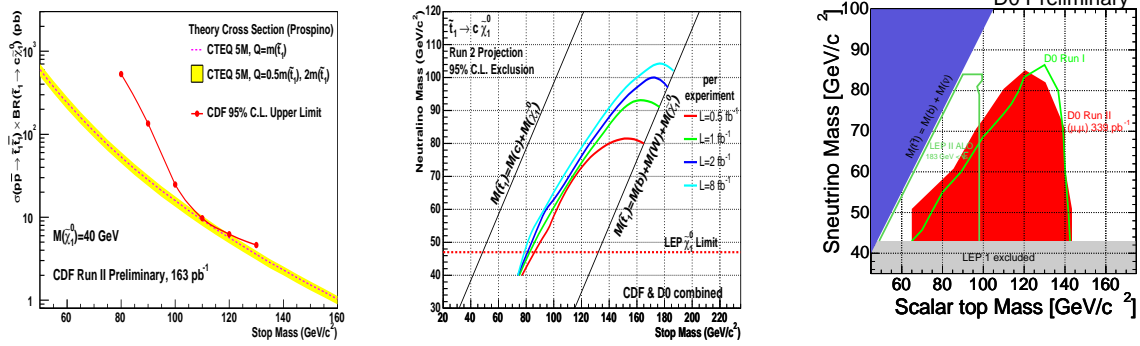


**Figure 33.** Left: CDF scalar top cross section limit. Center: CDF and DØ scalar top sensitivity reach. Right: DØ  $\tilde{t}_1\tilde{t}_1^* \rightarrow b\bar{b}\mu^+\mu^-\tilde{\nu}\tilde{\nu}$  limits. The dark region in the center is excluded at 95%CL.

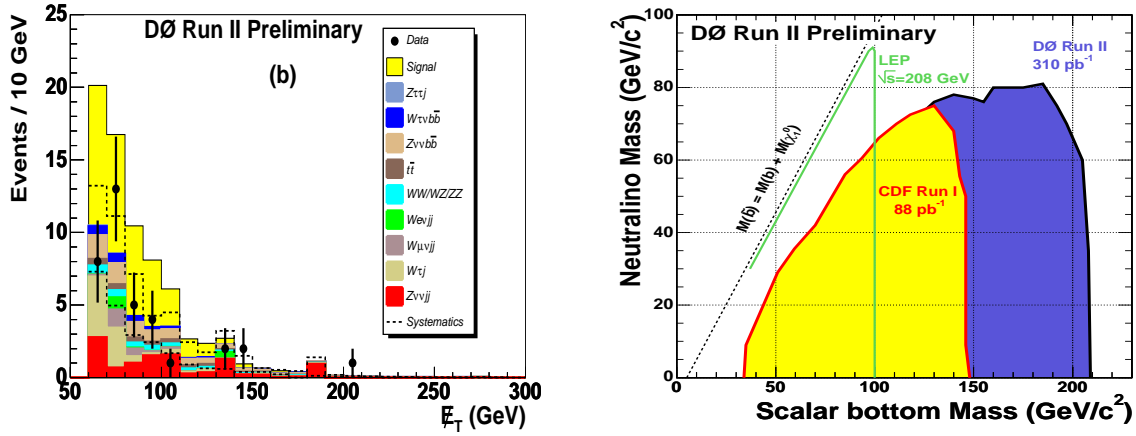


**Figure 34.** DØ. Left: sbottom missing  $E_T$  distribution. Right: sbottom-neutralino mass limits.

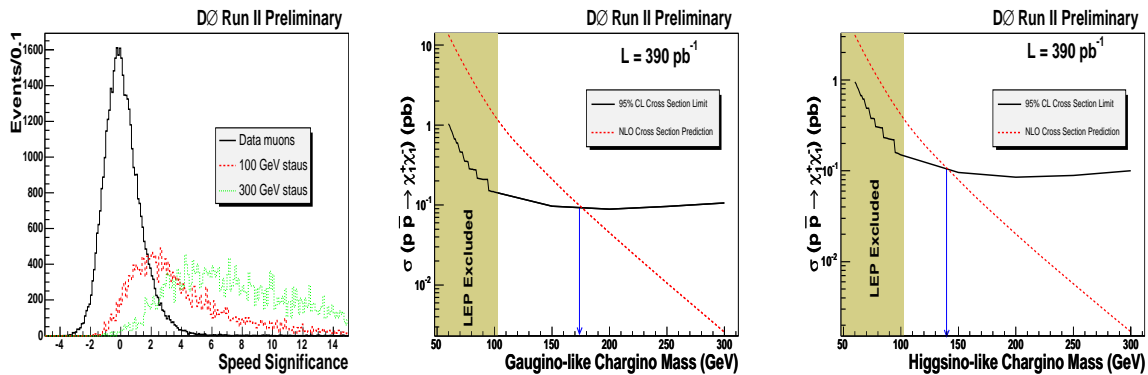


**Figure 35.** DØ. Left: speed significance of charged massive particle. Center: AMSB gaugino interpretation. Right: MSSM higgsino interpretation.

## 4. LHC Prospects

The LHC will operate at 14 TeV, which is about seven times the center-of-mass energy of the Tevatron. This important increase extends the reach to discover new particles. The first collisions at the LHC are scheduled for fall 2007, and the physics data run in 2008.

### 4.1. SM Higgs Boson

**4.1.1. Production and Decay** The search of the SM Higgs boson will consist of a variety of search channels, defined by the production and decay properties of the Higgs boson. The expected production cross sections and branching ratios are summarized in Fig. 36 (from [8] and [9]). The expected production cross sections for a 120 GeV Higgs boson are for the Tevatron (LHC):  $1.01 \text{ pb}^{-1}$  ( $42.1 \text{ pb}^{-1}$ ) gluon fusion,  $0.071 \text{ pb}^{-1}$  ( $4.41 \text{ pb}^{-1}$ ) vector boson fusion (VBF),  $0.153 \text{ pb}^{-1}$  ( $1.65 \text{ pb}^{-1}$ ) associated W production, and  $0.093 \text{ pb}^{-1}$  ( $0.89 \text{ pb}^{-1}$ ) associated Z production [8]. Thus, for this Higgs boson mass the expected rates are typically larger by a factor 10 to 40 at the LHC compared to the Tevatron.

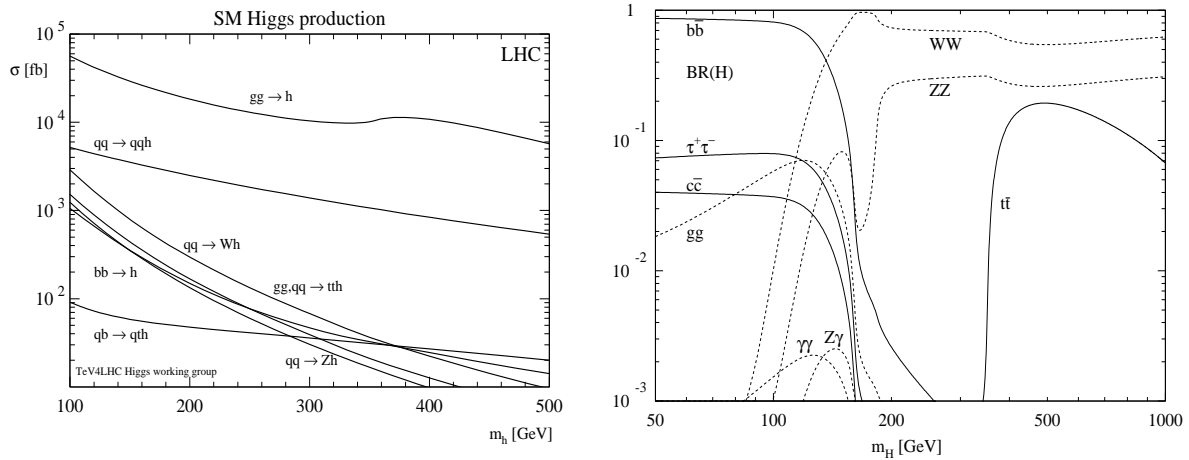


**Figure 36.** Left: expected SM Higgs boson production cross sections at the LHC (14 TeV). Right: expected Higgs boson decay branching ratios for a SM Higgs boson masses up to 1 TeV.

**4.1.2. Sensitivity Reach** For an integrated luminosity of  $30 \text{ fb}^{-1}$ , which is expected to be collected in 3 years of data-taking (2008-2010), the highest sensitivity for a SM Higgs boson with mass around 120 GeV SM Higgs boson is expected from the VBF process  $qqH$  ( $H \rightarrow \tau^+\tau^-$ ). The signal significances are summarized in Fig. 37 (from [50]). The strong potential to separate a 135 GeV signal from the background, which arises mainly from  $Z \rightarrow \tau^+\tau^-$ , is shown in Fig. 37 (from [51]). The LHC will be able to cover the full mass range of interest with  $10\text{-}30 \text{ fb}^{-1}$  and will give a definitive experimental answer on the existence of the Higgs boson mechanism.

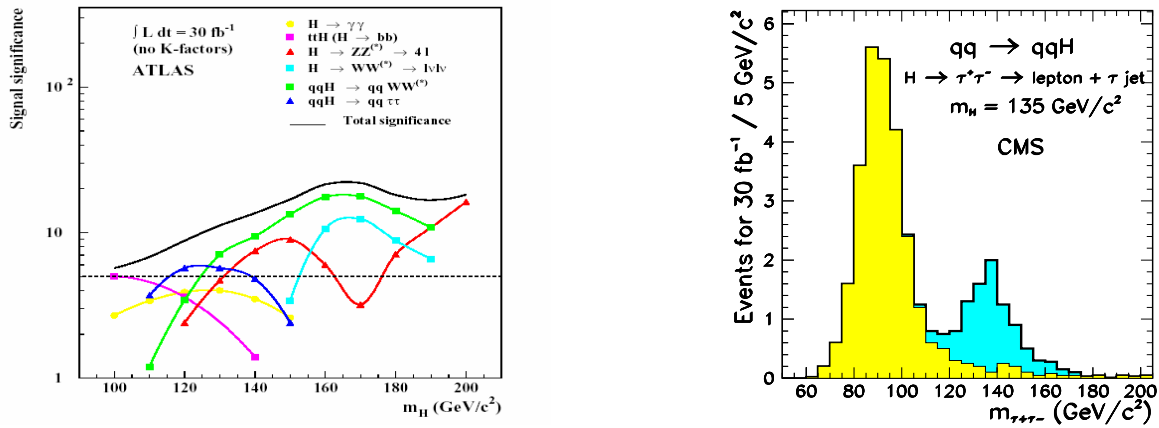


**Figure 37.** Left: ATLAS signal significance as a function of the SM Higgs boson mass. Right: CMS  $qqH (H \rightarrow \tau^+\tau^-)$  reconstructed invariant  $\tau^+\tau^-$  mass for simulated signal and background.

**4.1.3. Parameter Determination** First measurements of the SM Higgs boson branching ratios times production cross sections are expected already with a luminosity of  $10\text{--}30 \text{ fb}^{-1}$ . The precision depends on the Higgs boson mass, and on the luminosity uncertainty, as shown in Fig. 38 (from [53]) for  $300 \text{ fb}^{-1}$ . The figure shows also the precision on the SM Higgs boson coupling ratios. With an upper bound on the Higgs–gauge–boson couplings the absolute couplings rather than coupling ratios can be extracted as shown in Fig. 38 (from [54]). The expected precision on the measurement of the SM Higgs boson mass and its width is given in Fig. 39 (from [55]).

The spin and CP-value of the Higgs boson can be determined from studying the  $gg \rightarrow H \rightarrow ZZ \rightarrow 4\ell$  process, where the  $ZZ$  production is kinematically allowed. Figure 40 (from [56]) illustrates the sensitive variables and shows the clear separation between spin and CP values. A future Linear Collider will improve both the mass and width determination [52] and has in addition the potential to measure the Higgs boson self-coupling which is directly related to the shape of the Higgs boson potential.

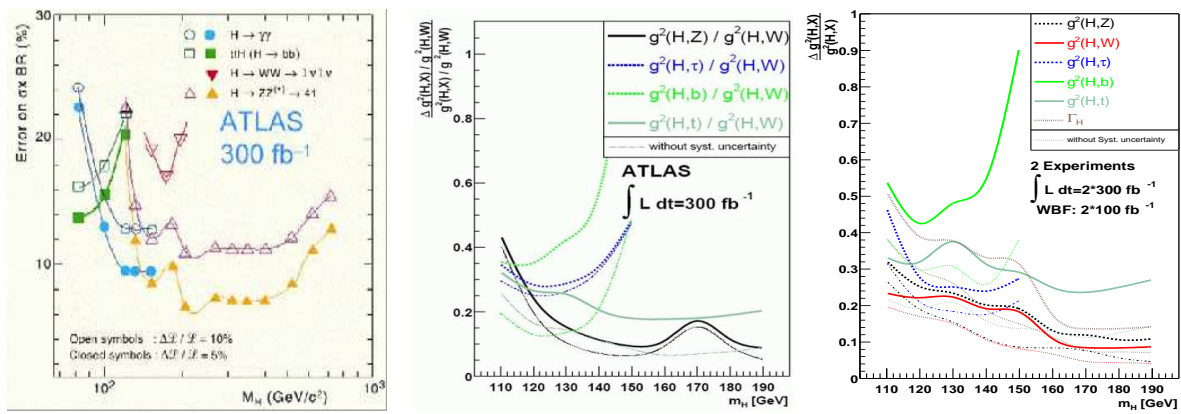


**Figure 38.** ATLAS. Left: expected precision on SM Higgs boson branching ratios times production cross sections. Center: expected precision on SM Higgs boson coupling ratios. Right: expected precision on SM Higgs branching ratios.



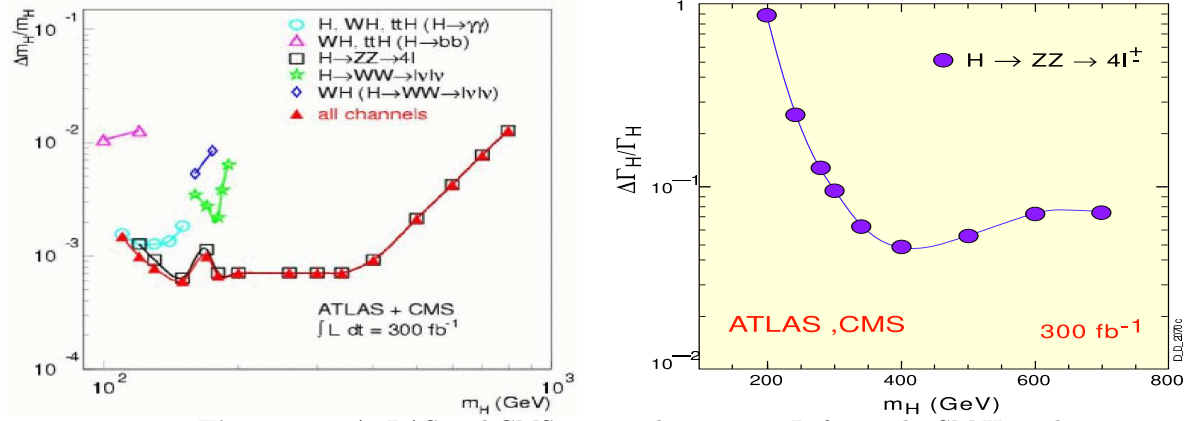


**Figure 39.** ATLAS and CMS expected precision. Left: on the SM Higgs boson mass. Right: on the SM Higgs boson width.

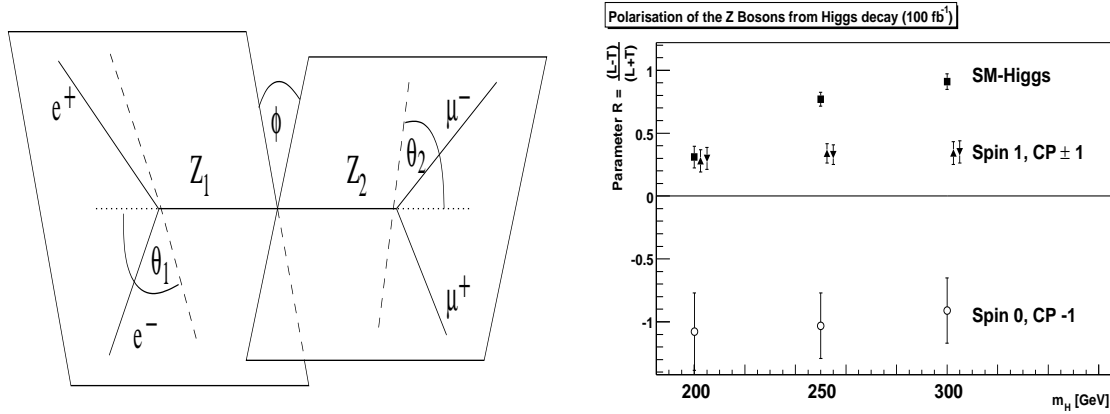


**Figure 40.** Left: angle  $\phi$  between the two planes defined by the leptons from the decay of the two Z bosons in the rest frame of the Higgs. The dashed lines represent the direction of motion of the leptons in the rest frame of the Z boson from which they originate. Angles  $\theta_1$  and  $\theta_2$  are between the negatively charged leptons and the direction of motion of the corresponding Z in the Higgs boson rest frame. Right: parameter  $R$ , related to the decay angles, for different Higgs boson masses. Spin and CP values can be well separated within the expected uncertainties.

## 4.2. Beyond the SM

**4.2.1. Invisibly Decaying Higgs Bosons** In models beyond the SM, the Higgs boson could decay invisibly, for example into a pair of neutralinos, as illustrated in Fig. 41 (from [57]). The parameter  $\xi$  is defined as  $g(hZZ)/g(H_{\text{SM}}ZZ)$ . The sensitivity at the LHC extends the LEP results [1].

**4.2.2.  $H \rightarrow \tau^+\tau^-$  and  $\tan\beta$  Determination** In the general 2-doublet Higgs model, the decay mode  $H \rightarrow \tau^+\tau^-$  is expected to be enhanced for large values of  $\tan\beta$ . A clear signal over the background will be obtained as shown in Fig. 42 (from [58]). The measurement of the expected rate will allow the determination of  $\tan\beta$  with the expected precision as given in Fig. 42. The precise determination of other SUSY parameters is an important requirement. Further measurable dependencies on  $\tan\beta$  of Higgs boson parameters have been discussed in the Linear Collider context [59].

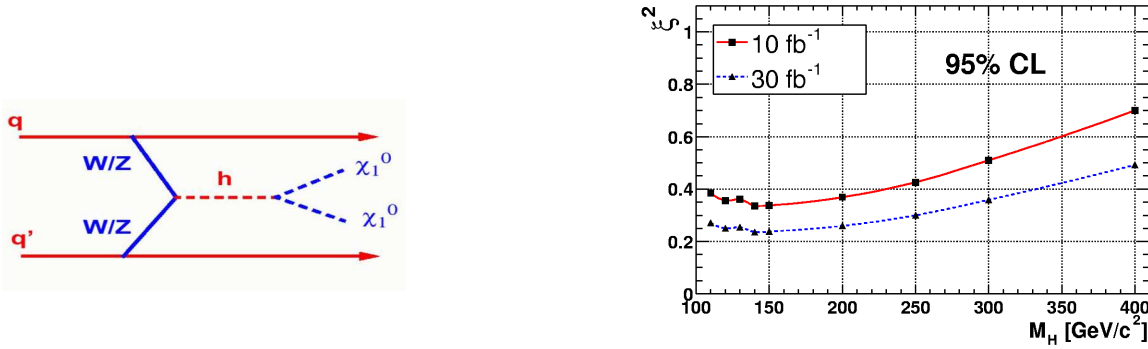


**Figure 41.** ATLAS invisibly decaying Higgs bosons. Left: production and decay graph. Right: sensitivity reach.

In the MSSM, the LHC will cover the entire  $(m_A, \tan\beta)$  parameter space and one or more Higgs bosons will be detected (Fig. 43 from [60]). For large  $\tan\beta$  several Higgs bosons are expected to be detected, while for medium  $\tan\beta$  values and  $m_A$  above about 200 GeV, only one SM-like Higgs boson is expected to be detected. In this region the determination of the underlying model is particularly challenging. Further measurements with higher precision to determine the underlying process will be possible at a future Linear Collider (for an overview see for example Ref. [61]).

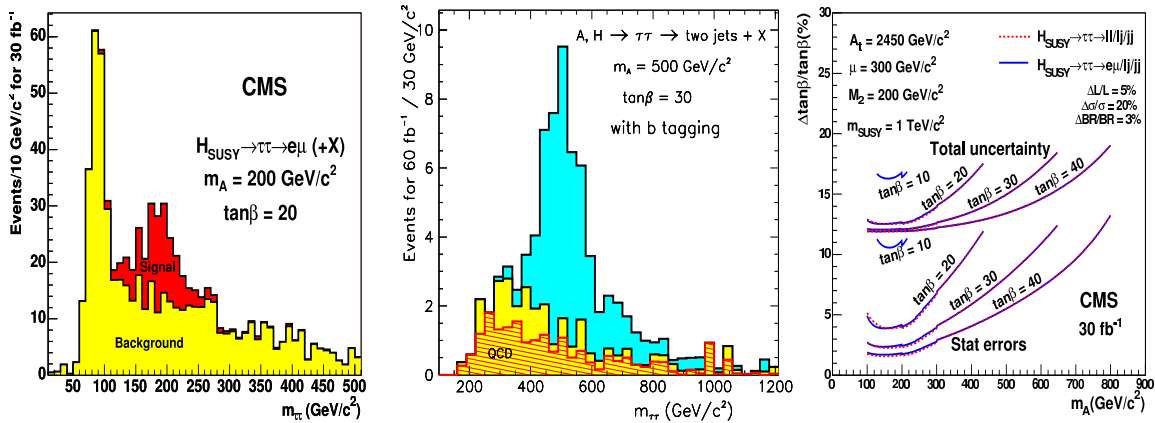


**Figure 42.** CMS. Left:  $H \rightarrow \tau^+\tau^- \rightarrow e\mu (+X)$  expected signal and background. Center:  $H \rightarrow \tau^+\tau^- \rightarrow \text{jets} (+X)$  expected signal and background. Right: expected sensitivity on  $\tan\beta$  including statistical and systematic uncertainties (upper lines).

### 4.3. Supersymmetric Particles

In searches for Supersymmetric particles, the LHC has the potential for a discovery within a short period of data-taking. An example in the mSUGRA model is shown in Fig. 44 (from [62]). A variety of Supersymmetric reactions will be in reach of the LHC. While a signature from Supersymmetry at the LHC cannot escape detection, measuring the underlying structure is a very challenging task. Further precision measurements will be possible at a Linear Collider, as reviewed for example in Ref. [63]. It will be particular difficult for the LHC to determine the relevant scalar top parameters in the cosmologically interesting region of stop-neutralino co-annihilation [64], where a future Linear Collider can perform precision measurements [46].

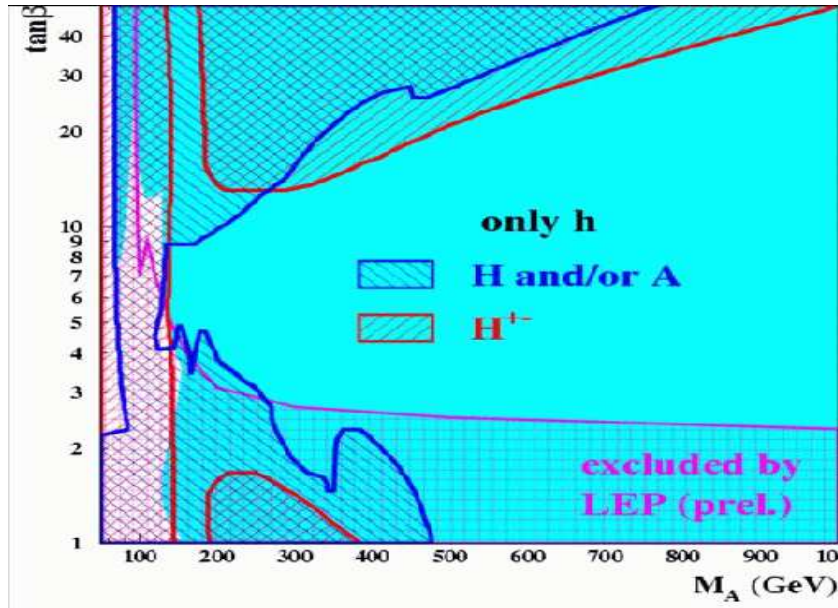


Figure 43. Expected parameter region of detection in the  $m_A$  versus  $\tan\beta$  plane of the MSSM for one or several Higgs bosons.

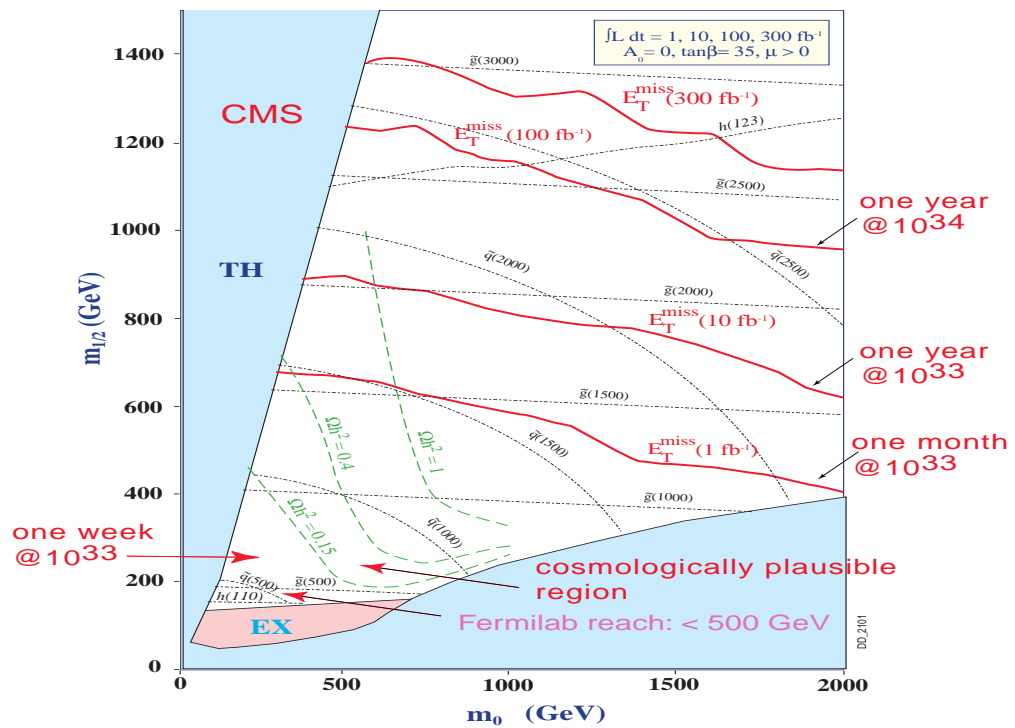


Figure 44. Squark-quino  $5\sigma$  discovery reach with a jets plus missing energy signal in the mSUGRA model. In the forbidden region on the left (small  $m_0$ ), the neutralino is not the LSP and in the lower region (small  $m_{1/2}$ ) there is no electro-weak symmetry breaking. The cosmologically plausible region is in particular near the forbidden region on the left (co-annihilation) and near the forbidden region near the bottom (focus-point). These regions could be covered within about the first year of data-taking. With a similar luminosity squarks of up to 2500 GeV could be discovered.

## 5. Conclusions

Much has been learned from the searches for Higgs bosons and other new particles at LEP. The Tevatron Run-II searches are well under way and already have set several limits exceeding the previous LEP limits. For the SM Higgs boson, searches for gluon fusion with WW decays, associated production WH with  $b\bar{b}$  and WW decays, and  $ZH \rightarrow \nu\nu b\bar{b}$  decays have been performed. Beyond the Standard Model, the searches at the Tevatron for  $bbA$ ,  $H^{++}$ ,  $h \rightarrow \gamma\gamma$ , and  $\tau^+\tau^-$  have also much more potential for a discovery with larger luminosity. In Supersymmetry, searches for neutralinos and charginos in GMSB and mSUGRA models, as well as searches for squark and gluino, scalar tops, scalar bottoms, and scalar taus already have set new limits. In the near future, the LHC will extend the discovery reach in the Higgs sector, and has also the potential to measure the masses, branching ratios and  $\tan\beta$ . Supersymmetric particles could be discovered in a short time of operation after detector calibration and a good understanding of the SM backgrounds. With the operation of the Tevatron at increasing data rates and the LHC ahead, it is an exciting time for new discoveries. The close collaboration of phenomenologists and experimentalists is crucial to fully exploit the potential of the current and future accelerators.

## Acknowledgments

I like to thank the organizers of PHENO'05 and the organizers of the workshop 'From the Tevatron to the LHC to the Linear Collider' at the Aspen Center for Physics'05 for their invitation and the very kind hospitality. I would also like to thank Gregorio Bernardi, Suyong Choi and Arnd Meyer from the DØ experiment, Song Ming Wang and Tom Junk from the CDF experiment, Steve Mrenna from the Fermilab Theory and Computing Division, and Albert de Roeck from the LHC for comments on the manuscript.

## References

- [1] A. Sopczak, Proceedings QFTHEP'04, St. Petersburg, Russia; and WONP'05, Havana, Cuba, hep-ph/0502002.
- [2] A. Sopczak, "MSSM Higgs boson searches at LEP", Talk at the 13th International Conference on Supersymmetry and Unification of Fundamental Interactions (SUSY'05), Durham, UK, July 18-23, 2005, hep-ph/0602136.
- [3] The Tevatron Electroweak Working Group, and the CDF and DØ Collaborations, hep-ex/0507091.
- [4] The LEP Electroweak Working Group, <http://lepewwg.web.cern.ch/LEPEWWG>, hep-ex/0511027.
- [5] Fermilab Operations, <http://www-bdnew.fnal.gov/operations/lum/lum.html>.
- [6] M. Carena et al., "Report of the Tevatron Higgs working group", hep-ph/0010338.
- [7] L. Babukhadia et al., "Results of the Tevatron Higgs Sensitivity Study", FERMILAB-PUB-03/320-E.
- [8] F. Maltoni et al., <http://maltoni.home.cern.ch/maltoni/TeV4LHC/SM.html>.
- [9] A. Djouadi, J. Kalinowski and M. Spira, *Comput. Phys. Commun.* **108** (1998) 56.

- [10] G. Busetto, J. Donini, T. Dorigo, M. Shochet and C. Neu, CDF Collaboration, “Z  $\rightarrow$   $b\bar{b}$  Analysis”, public note, Feb. 18, 2005; <http://www-cdf.fnal.gov/physics/exotic/r2a/20050218.zbbbar>.
- [11] V. M. Abazov et al., DØ Collaboration, Phys. Rev. Lett. **94**, 161801 (2005).
- [12] C. S. Hill, CDF Collaboration, Nucl. Instrum. Meth. **A530** (2004) 1.
- [13] A. Melnitchouk, DOE review University of Mississippi, February 9, 2005.
- [14] I. Iashvili, TeV4LHC Workshop, Fermilab, Chicago, October 2005.
- [15] A. Haas, “A Search for Neutral Higgs Bosons at High  $\tan\beta$  in Multi-jet Events from  $p\bar{p}$  Collisions at  $\sqrt{s} = 1960$  GeV”, University of Washington, PhD Thesis (2005).
- [16] CDF Collaboration, CDF/PUB/EXOTIC/PUBLIC/7893, Dec. 20, 2004.
- [17] V. M. Abazov et al., DØ Collaboration, Phys. Rev. Lett. **96**, 011801 (2006).
- [18] DØ Collaboration, DØ note 4896-CONF, May 18, 2005;  
V. M. Abazov et al., DØ Collaboration, Phys. Rev. Lett. **94**, 091802 (2005).
- [19] CDF Collaboration, CDF/PUB/EXOTIC/7740, July 5, 2005.
- [20] DØ Collaboration, DØ note 4861-CONF, July 5, 2005.
- [21] CDF Collaboration, CDF/PUB/EXOTIC/7307, October 24, 2005.
- [22] DØ Collaboration, DØ note 4774-CONF, April 14, 2005.
- [23] CDF Collaboration, CDF/PUB/EXOTIC/7983, Dec. 13, 2005.
- [24] CDF and DØ Collaborations, <http://www-cdf.fnal.gov/physics/exotic/exotic.html> and <http://www-d0.fnal.gov/Run2Physics/WWW/results/higgs.htm>.
- [25] G. Bernardi, TeV4LHC Workshop, Fermilab, Chicago, October 2005.
- [26] A. Belyaev, T. Han and R. Rosenfeld, JHEP **307** (2003) 21.
- [27] J. Campbell, R. K. Ellis, F. Maltoni and S. Willenbrock, Phys. Rev. D **67**, 095002 (2003).
- [28] S. Dawson, C. B. Jackson, L. Reina and D. Wackerroth, Phys. Rev. D **69**, 074027 (2004);  
S. Dittmaier, M. Krämer and M. Spira, Phys. Rev. D **70**, 074010 (2004).
- [29] V. M. Abazov et al., DØ Collaboration, Phys. Rev. Lett. **95**, 151801 (2005).
- [30] T. Affolder et al., CDF Collaboration, Phys. Rev. Lett. **86**, 4472 (2001).
- [31] CDF and DØ collaborations, <http://www-cdf.fnal.gov/physics/projections> (Sep. 2005).
- [32] A. Abulencia et al., CDF Collaboration, hep-ex/0508051 (2005), FERMILAB-PUB-05-374-E, August 2005.
- [33] CDF Collaboration, CDF/PUB/EXOTIC/7712, June 23, 2005.
- [34] DØ Collaboration, DØ note 4374-CONF, March 18, 2004.
- [35] D. Acosta et al., CDF Collaboration, Phys. Rev. Lett. **95**, 071801 (2005).
- [36] V.M. Abazov et al., DØ Collaboration, Phys. Rev. Lett. **93**, 141801 (2004).
- [37] DØ Collaboration, DØ notes 4737-CONF, March 3, 2005.
- [38] CDF Collaboration, Large  $H_t$  event, CDF/PUB/EXOTIC, 2005, <http://www-cdf.fnal.gov/physics/exotic/exotic.html>.
- [39] LEPSUSYWG, ALEPH, DELPHI, L3 and OPAL experiments, <http://lepsusy.web.cern.ch/lepsusy>.
- [40] F. Abe et al., CDF Collaboration, Phys. Rev. Lett. **81**, 1791 (1998).
- [41] V. M. Abazov et al., DØ Collaboration, Phys. Rev. Lett. **94**, 041801 (2005).
- [42] V. Büscher et al., CDF and DØ Collaborations, hep-ex/0504004.
- [43] DØ Collaboration, DØ notes 4740-CONF, 4741-CONF, 4742-CONF, March 2, 2005.
- [44] DØ Collaboration, Tri-lepton expectations, [http://www.fnal.gov/directorate/program\\_planning/studies/projections09\\_06\\_05.htm](http://www.fnal.gov/directorate/program_planning/studies/projections09_06_05.htm).
- [45] CDF Collaboration, CDF/PUB/EXOTIC/7458, January 30, 2005.
- [46] M. Carena, A. Finch, A. Freitas, C. Milstene, H. Nowak and A. Sopczak, hep-ph/0508152, in press Phys. Rev. D.
- [47] DØ Collaboration, DØ notes 4866-CONF, July 12, 2005.
- [48] DØ Collaboration, DØ notes 4832-CONF, June 28, 2005.
- [49] DØ Collaboration, DØ notes 4746-CONF, March 3, 2005.
- [50] S. Asai et al., ATLAS note ATL-PHYS-2003-005, April 18, 2003;

- S. Asai et al., Eur. Phys. J. C **32S2** (2004) 19.
- [51] R. Kinnunen, K. Lassila-Perini, S. Lehti, P. Salmi with S. Abdullin et al., CMS NOTE-2003/033, December 10, 2003.
- [52] V. Drollinger and A. Sopczak, Eur. Phys. J. directC **3**, N1 (2001).
- [53] M. Dürrssen, ATLAS note Phys-2003-030.
- [54] M. Dürrssen, S. Heinemeyer, H. Logan, D. Rainwater, G. Weiglein and D. Zeppenfeld, hep-ph/0407190.
- [55] L. Zivkovic, Czech. J. Phys. **54** (2004) 73.
- [56] C. P. Buszello, I. Fleck, P. Marquard and J. J. van der Bij, Eur. Phys. J. C **32** (2004) 209.
- [57] L. Neukermans and B. Di Girilamo, ATLAS note ATL-PHYS-2003-006, April 14, 2003; O. J. P. Eboli and D. Zeppenfeld, Phys. Lett. B **495**, 147 (2000).
- [58] R. Kinnunen, S. Lehti, F. Moortgat, A. Nikitenko and M. Spira, Eur. Phys. J. C **40** N5 (2005) 23.
- [59] J. F. Gunion, T. Han, J. Jiang and A. Sopczak, Phys. Lett. B **565**, 42 (2003).
- [60] M. Schumacher, “Investigation of the discovery potential for Higgs bosons of the minimal supersymmetric extension of the standard model (MSSM) with ATLAS”, Talk at the 12th International Conference on Supersymmetry and Unification of Fundamental Interactions (SUSY’04), Tsukuba, Japan, 17-23 June 2004; hep-ph/0410112.
- [61] A. Sopczak, “Higgs physics at a high luminosity  $e^+e^-$  Linear Collider,” ICHEP’02, hep-ph/0209372, Proc. *North Holland Elsevier* (2003) p. 241.
- [62] F.E. Paige, “SUSY signatures at LHC”, Talk at the 10th International Conference on Supersymmetry and Unification of Fundamental Interactions (SUSY’02), Hamburg, Germany, 17-23 Jun 2002, hep-ph/0211017.
- [63] A. Sopczak, “Exploring Supersymmetry at a Future Global  $e^+e^-$  Linear Collider”, Talk at the 11th International Conference on Supersymmetry and Unification of Fundamental Interactions (SUSY’03), Supersymmetry in the Desert, University of Arizona, Tucson, June 5-10, 2003, hep-ph/0403087.
- [64] I. Borjanovi, “SUSY Signatures with ATLAS”, HEP2005, Lisbon, 21-28, July, 2005; [http://atlas.web.cern.ch/Atlas/GROUPS/PHYSICS/Conferences/2005/HEPP-EPS05\\_Borjanovic.pdf](http://atlas.web.cern.ch/Atlas/GROUPS/PHYSICS/Conferences/2005/HEPP-EPS05_Borjanovic.pdf)
- .